

Metamodel techniques to estimate the compressive strength of UHPFRC using various mix proportions and a high range of curing temperatures

Wael Emad^a, Ahmed Salih Mohammed^{b,*}, Ana Bras^c, Panagiotis G. Asteris^d, Rawaz Kurda^{e,f,g,*}, Zhyan Muhammed^h, A.M.T. Hassanⁱ, Shaker M.A. Qaidi^j, Parveen Sihag^k

^a Department of Civil Engineering, Komar University, Iraq

^b Civil Engineering Department, College of Engineering, University of Sulaimani, Iraq

^c Built Environment and Sustainable Technologies (BEST) Research Institute, Liverpool John Moores University, United Kingdom

^d Computational Mechanics Laboratory, School of Pedagogical and Technological Education, Heraklion, 14121 Athens, Greece

^e Department of Highway and Bridge Engineering, Technical Engineering College, Erbil Polytechnic University, Erbil 44001, Iraq

^f Department of Civil Engineering, College of Engineering, Nawroz University, Duhok 42001, Iraq

^g CERIS, Civil Engineering, Architecture and Georesources Department, Instituto Superior Técnico, Universidade de Lisboa, Av. Rovisco Pais, 1049-001 Lisbon, Portugal

^h Civil Engineering Department, College of Engineering, University of Sulaimani, Iraq

ⁱ The American University of Iraq, Sulaimani (AUIS), Sulaimani, Kurdistan Region

^j Department of Civil Engineering, College of Engineering, University of Duhok, Duhok, Kurdistan-Region, Iraq

^k Civil Engineering Department, Shoolini University, Solan, Himachal Pradesh, India



ARTICLE INFO

Keywords:

Ultra-high performance fiber reinforced concrete (UHPFRC)
Compressive strength
Durability
Curing condition
Soft computing
Statistical evaluation

ABSTRACT

In order to predict the compressive strength (σ_c) of Ultra-high performance fiber reinforced concrete (UHPFRC), developing a reliable and precise technique based on all main concrete components is a cost-effective and time-consuming process. To predict the UHPFRC compressive strength, four different soft computing techniques were developed, including the nonlinear- relationship (NLR), pure quadratic, M5P-tree (M5P), and artificial neural network (ANN) models. Thus, 274 data were collected from previous studies and analyzed to evaluate the effect of 11 variables that impact the compressive strength, including curing temperature. The performance of the predicted models was evaluated using several statistical assessment tools. According to the findings, ANN results performed more suitable than other models with the lowest root mean square error (RMSE) and highest coefficient of determination (R²) value. According to the sensitivity analysis, the most variables that affect the compressive strength prediction of UHPFRC are a curing temperature with a percentage of 17.36%, the fiber content of 17.13%, and curing time of 15.13%.

1. Introduction

Increasing demand for concrete to provide a durable, blast resistance, and safe structure is further developed. One symbol of every city's development is the number of strategic, modern, and high-rise buildings, but using concrete to protect such structures from environmental and technical hazards such as earthquakes, terrorist attacks, explosions, and plane impact is essential. The UHPFRC is the ideal selection since it provides a very high compressive strength, high tensile strength due to the inclusion of fiber, very low permeability, and less dimension [1]. This new type of concrete is specified by a high content of cement which

is about two times more than common concrete, high fiber content, fine sand with particle sizes less than 1 mm, water/cement ratio ranging between 0.16 and 0.23, superplasticizer, high ratio of fiber normally 12 mm length and 0.2 mm diameter [2–6]. The concrete packing is densified by replacing cement with pozzolanic materials or mineral admixtures such as; Silica fume (SF), Nano silica, Pulverized fly ash, and Metakaolin [7–9]. When studying the impact of water content on the mechanical and flowability of UHPFRC, Corinaldesi and Moriconi [10] observed several mixes after keeping the cement, superplasticizer, and silica fume, and sand content constant with different water to binder ratios (up to 0.32). They claimed that 0.24 produced the optimum

* Corresponding authors at: Department of Highway and Bridge Engineering, Technical Engineering College, Erbil Polytechnic University, Erbil 44001, Iraq (Rawaz Kurda).

E-mail addresses: wael.mahmood@komar.edu.iq (W. Emad), ahmed.mohammed@univsul.edu.iq (A.S. Mohammed), Rawaz.Kurda@tecnico.ulisboa.pt (R. Kurda), shaker.abdal@uod.ac (S.M.A. Qaidi).

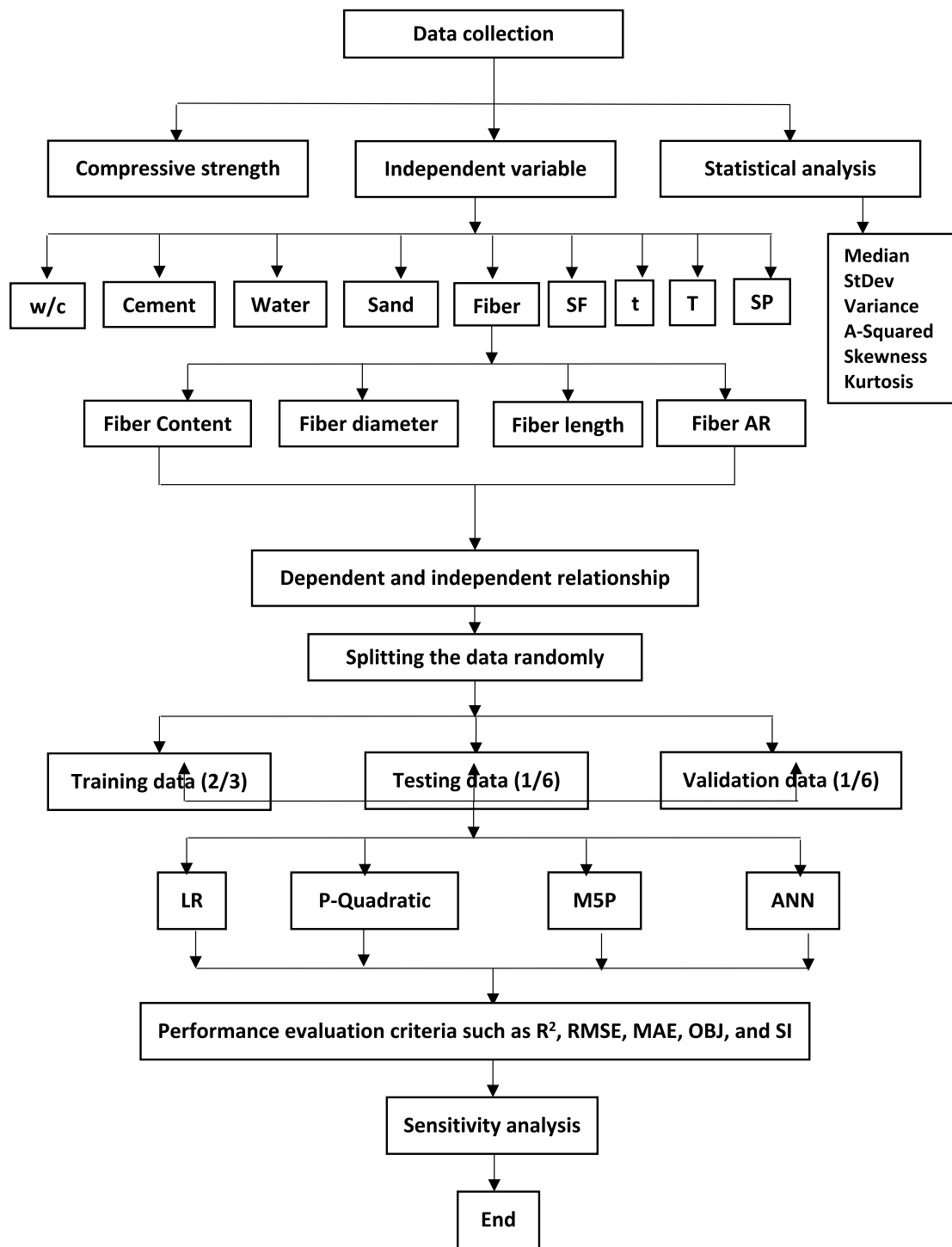


Fig. 1. The flow chart diagram for the current study's procedure.

mechanical and flowability for concrete mixes. The type and size of the sand particle are essential when preparing UHPFRC samples to reduce the overall cost of producing UHPFRC samples. Yang et al. [5] studied the impact of replacing silica sand with two natural sand and with Recycled Glass Cullet (RGC). The final results proved that the flowability of the mixture was reduced by using angular particles. Both natural grains of sand can be used as a silica sand replacement without losing mechanical and ductility properties, but RGC decreased the flexural and compressive strengths by 15 %. Most of the research focused on preparing UHPFRC at an elevated temperature since it provided high strength in a short duration of curing; as an attempt to bring and use

UHPFRC in site construction applications. Hassan et al. [11] investigated the mechanical performance of UHPFRC and indicated that at early testing ages, to develop the strength properties curing temperature is crucial. Several samples were cast and cured at curing temperatures ranging between 10 and 90 °C for up to one year and compared the results of low curing with high curing temperature. Maximum compressive and flexural strength were measured at 7 days for 90 °C curing specimens, but similar strength was obtained for specimens cured at low temperature only after 90 days of curing.

Yang et al. [5] stated that concrete samples cured at 90 °C for 7 days recorded 80, 90, and 90 % higher compressive, flexural strength, and

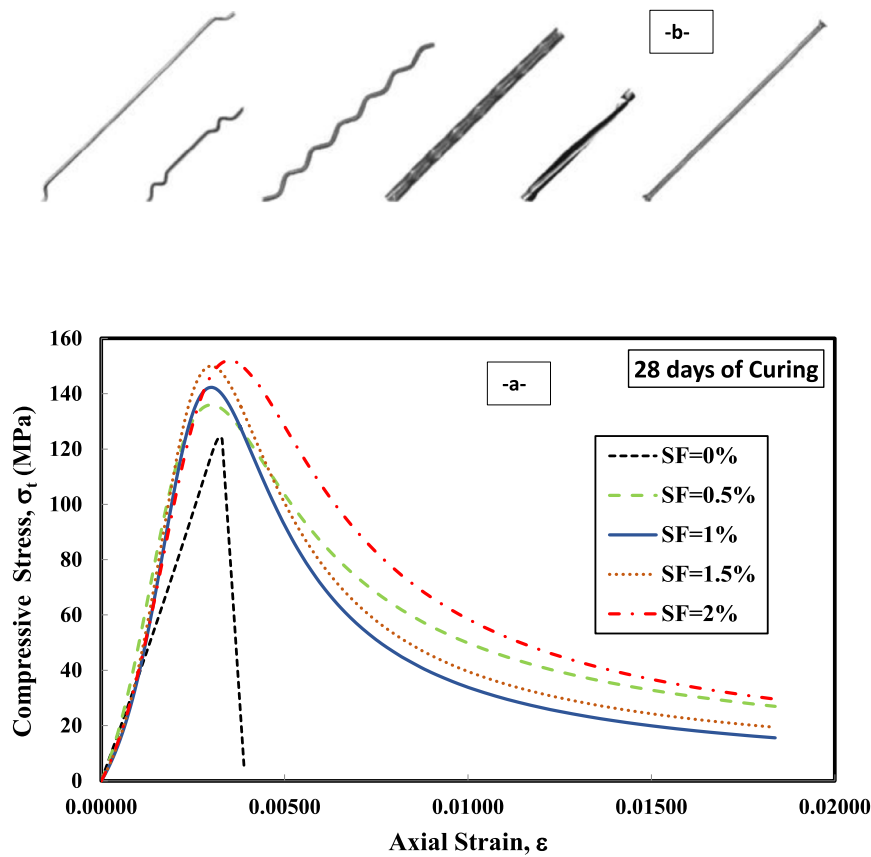


Fig. 2. (a) Compressive stress–strain curves concerning the steel fiber content (SF %) on the 28 days of curing and (b) Different types of steel fibres [11].

fracture energy, respectively than samples cured at the same time at 20 °C. Magureanu et al. [12] cured several samples using two different curing regimes, water curing at 20 °C, and ii) thermal curing at 90 °C for 5 days; after testing all specimens at the age of 6 days, they observed an increase in both compressive and flexural strength up to 181, and 17.5 MPa respectively but the results were less than 130, and 6 MPa for the compressive strength and the tensile strength of the same samples cured in water at 20 °C.

When fibers are incorporated, UHPC is called Ultra-High Performance Concrete Reinforced with Fibers (UHPFRC) [12]. Irrespective of its size, type, and shape, the fibers have a key role in enhancing the confrontation of plain UHPC to cracking, ductility, and toughness properties. In UHPFRC, fibers have the potential to promote energy absorption, strain hardening under tension, and avoid sudden failure. Microfibers from different resources, including steel, glass, and carbon, are usually employed to produce UHPFRC. To determine fracture energy, inverse analysis can be utilized to classify it, but this needs to utilize a particular test program and numerical methods [18]. UHPFRC is usually characterized by ultimate strength, superior fracture parameters, and enhanced durability if proper manufacturing techniques (water, steam, or autoclave curing) are adopted. Steam curing for UHPC is very effective because it enhances the hydration of large amounts of un-hydrated cement inside UHPCs due to large quantities of binder, but it also helps in controlling the moisture movement from and into the concrete [11,12]. Therefore, researchers preferred steam over water curing to produce UHPFRCs, and superior results were obtained. For instance, steam curing of concrete at atmospheric pressure results in a considerable increment in the strength development rate. This method is mainly used for prefabricated concrete parts such as pipes and pre-stressed elements; nonetheless, it can also be used for closed in situ constructions. In the manufacturing of precast concrete elements, steam

curing enables higher production through faster turnover mold and formwork, shorter curing times before shipping, and less product damage during transport. The pozzolanic reaction, which is thermally activated due to the high curing temperature of steam curing, leads to the growth of C—S—H and a decrease in calcium hydroxide [13,14].

The influence of the curing temperature on the properties of cement mortars and concretes was the focus of some studies. It has been largely clarified that curing at a high temperature immediately after casting provides the growth of mechanical characteristics in the initial ages. It adversely affects strength in the final ages. At 28 days, a 10 % reduction in compressive strength was detected when the concrete was cured at 35 °C, related to the concrete cured at 20 °C. Furthermore, with increasing the curing regime from 20 and 50 °C, the strength decreased by 28 %. This drop-down of strength in later age refers to the sudden hydration rate in early ages due to the higher temperature, which delays the consequent hydration and forms a non-uniform distribution of the hydration products [14]. The possible benefits of steam curing of concrete with the combination of fly ash, slag, and silica fume. It was obtained that mixtures with silica fume (SF) provided a good strength performance and low sorptivity at an early age [14]. The UHPC at 28 days cured in ambient condition showed a compressive strength of 126 MPa and tensile strength of 6.5 MPa. Further studies are required to implement different curing methods of UHPC to investigate the development strength at different ages. For this purpose, in the current study, water curing (WC) and steam curing (SC) were applied to produce UHPC based on blended binders such as cement and SF [12–14].

The benefits of using silica fume (SF) in concrete mixes include: improving compressive strength, bond strength, and wear resistance; additionally, the resistance against permeability and the corrosion resistance of the embedded is improved [27]. In the cementitious matrix, SF is the most widely used amorphous silica. The average particle



Fig. 3. Failure path of the concrete in two different shapes (a & c) UHPC (without steel fiber) and (b & d) UHPFRC (with steel fiber) [11].

size of SF is approximately-one-tenth that of cement. SF has been utilized in the range of 10–25 % by weight of cement since the 1950 s due to its Pozzolans and filler properties that make the concrete denser [8]. SF and calcium hydroxide react together to make more C—S—H gel, improving the final strength [9].

Furthermore, some investigators, such as Dunster [10], stated that the contributions of SF and concrete components could minimize cement consumption, which has become sustainable for economic and environmental development. Various studies have been implemented on the effects of different parameters, including fibers, mineral admixtures, and curing conditions, on the behavior of UHPFRC. For instance, the effects of various types of fibers on the mechanical performance and ductility behavior cured in water have been studied by researchers [28,29]. For this purpose, a w/b of 0.195 and different types of fiber content ranging between 0.25 and 2 % fiber volume fraction were used. It was concluded that the maximum compressive strength was 180 MPa for the micro steel fibers (MSF) and that, for flexural strength, the hooked steel fibers were more effective [30].

Moreover, the effects of nano-silica and micro-silica on the mechanical properties for the 0.2 w/b of UHPC were also investigated [14]. It was also detected that nano-silica and micro-silica binary usage provides superior performance to individual utilization. Maleka et al. [20] investigate UHPFRC using blended cement and SF. The cement content chosen in this research was 700, 750, and 800 kg/m³, and SF content of

0, 15, and 30 % of cement content. The study has recommended the inclusion of the SF of up to 30 % of cement content.

Also, the mechanical properties under different curing regimes containing mineral admixtures. They revealed that steam and autoclave curing looked like very effective ways to improve the strengths of UHPCs. However, there is very limited research on investigating the optimum content of binder and its effect on the mechanical and fracture parameters of UHPFRC cured via different methods. As a result of reviewing the available literature, the question of how to find the optimum balance between the binder content and aggregate volume to improve the performance of UHPC has become our main concern to find an answer. Therefore, an experimental program is prepared by taking different volumes of binder ranging between 850 and 1200 kg/m³ with an augmentation of 50 kg/m³ for investigating the strength and fracture parameters of UHPFRC. Moreover, the effect of curing methods (WC and ST) on the UHPFRCs was considered. Furthermore, parameters such as flowability of concrete, w/b ratio, SF, and MSF content were kept constant, unlike the binder content and curing methods (steam curing and water curing) which were varied for optimization purposes of the results of compressive strength, splitting strength, modulus of elasticity, flexural strength, load-displacement curves, fracture energy, and characteristic length [13].

To provide necessary dataset required for establishing the model, 50 dynamic load tests were conducted on precast concrete piles in

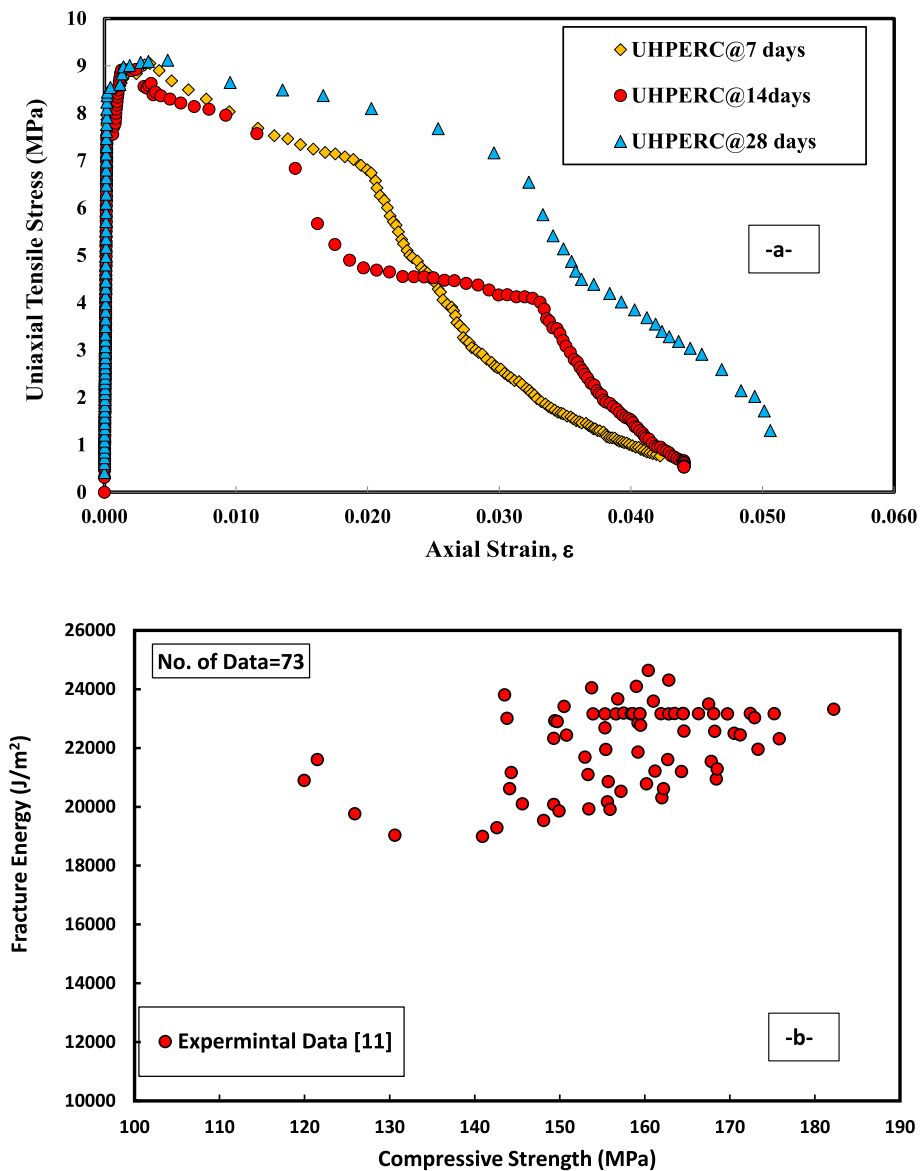


Fig. 4. (a) Direct tensile stress-strain curves concerning the steel fiber content (SF %) at different curing times and (b) the relationship between compressive strength and fracture Energy of UHPFRC [11].

Pekanbaru, Indonesia. The pile geometrical properties, pile set, hammer weight, and drop height were set to be the network inputs, and the pile ultimate bearing capacity was set to be the output of the GA-based ANN model. The best predictive model was selected after conducting a sensitivity analysis to determine the optimum GA parameters and a trial-and-error method for finding the optimum network architecture, i.e., the number of hidden nodes. Results indicate that the pile bearing capacities predicted by GA-based ANN align with measured bearing capacities. Coefficient of determination and mean square error equal to 0.990 and 0.002 for testing datasets, respectively, suggest that implementation of GA-based ANN models as a highly reliable, efficient, and practical tool in predicting the pile bearing capacity is of advantage [19]. An artificial neural network (ANN) is considered an AI technique that can forecast almost all problems in science and engineering fields [20]. However, they have several limitations discussed and introduced in previous research [22–24]. As stated in several references [19–21], the use of efficient optimization algorithms (OAs) can overcome these limitations. Various optimization algorithms such as the genetic algorithm (GA), particle swarm optimization (PSO), artificial bee colony (ABC), and imperialist competitive algorithm (ICA) can be used to solve

continuous and non-continuous problems. Due to the high ability of the global search for these OAs, weights, and deviations of an ANN can be determined to improve its performance forecast. The hybrid mentioned above models has been widely used to solve nonlinear and complex engineering problems [17–20].

1.1. Research objectives

This study aims to assess the impact of different mixture proportions and curing temperatures on the compressive strength of UHPFRC. For this reason, various modeling techniques such as Linear, Pure quadratic, M5P-tree, and ANN were performed using 274 data samples collected from previous research. The flowchart in Fig. 1 shows the procedure of this study. The main objectives of this research are:

- to perform a statistical study and evaluate the impact of different mixture compositions of UHPFRC on the compressive strength.
- to examine and design a reliable model for estimating the compressive strength among all models (linear, pure quadratic,

Table 1

Summary of different UHPFRC mixtures.

Ref.	w/c	C (kg/m ³)	S (kg/m ³)	SP (kg/m ³)	SF (kg/m ³)	t (day)	F (kg/m ³)	Fiber AR	T (°C)	σ_c (MPa)
[2]	0.3	657	1051	40	119	7–180	157	65	10–90	101.6–168
[4]	0.25	1092–1280	292–647	30.2–77.2	273–320	28	0–468	63.50	60	124–162
[5]	0.18	657	1050	1.05	119.4	7–56	156	65	20, 90	120–177
[10]	0.24–0.32	960	960	24	240	7, 28	192	72	20	100–147
[13]	0.25	1500	650	40	175	7–28	0–188	60, 120	28	93–118
[16]	0.22	784–809	1045–1079	20.9–21.6	261–270	3–90	0–234	65.00	20	93–166
[20]	0.26	700	1104	30	50	28	0–78	65	20	105–138
[21]	0.15	712	1020	30.7	231	3–56	156	62.5	60, 90	139–186
[22]	0.2	850	850	76.5	226	28	78–157	65	20	145–150
[23]	0.28	657	1051	40	119	7–28	157	65	90	145–150
[24]	0.23–0.33	612–874	1273.4	45.9	43.7	7, 28	39–195	65	21	99–156
[25]	0.21	1050	678	42	350	5	0–117	60	80	107–140
[26]	0.18	800	1250	80	240	7, 28	40	16.25	25	120–149
[27]	0.35	413	1593–1827	9.75	32.5	28	0–234	50	20	114–128
[28]	0.14–0.16	998.8	898–1014	49.4–88.2	176.25	7–28	0–78	722	21	112–160
[29]	0.2	1163–1543	607–1923	34.1–89.7	5.5–20	28	0–468	0–63.5	60, 90	131–169
[30]	0.20	788	795.88	14.77	197	28	157	81	200	140–171
[31]	0.35–0.36	641–648	943–952	34.2–45.6	40–41	28	312–390	65	23	146–150
[32]	0.22	788	867	14.77	197	28	0	0	20	132
[33]	0.19	720	1025	30.00	240	28	0–157	63.50	22	112–149
[34]	0.22	800	896–1056	39.00	200	28	80–240	59.00	21	150–152
[35]	0.25	900	826	36.00	225	56	0–156	60.00	25, 200	145–184
[36]	0.18	900	764–1055	40	44–220	28	157	85	22	125–161
[37]	0.16–9.22	703–950	690	24.5–28.5	285	28	0–117	0–1014	21, 125	101–178
[38]	0.24	900	1125	27	180–270	7, 28	0–154.8	380.79	2	90–136.6
Ranged between	0.14–0.36	413–1543	292–1923	1.05–89.7	5.5–350	3–180	0–468	0–1014.29	10–200	90.18–186

M5P-tree, and ANN models) using appropriate statistical evaluation tools.

(iii) Compare and quantify the most reliable model to estimate the compressive strength of UHPFRC.

1.2. Effect of steel fiber content on compressive strength

The concretes have reached their ultimate strength within 7 days, similar to their tensile strength [11]. The effect of steel fiber content on the stress-strain behavior of UHPC is presented in Fig. 2. This is due to the curing regime of the elevated temperature of 90 °C. Furthermore, the elastic behavior for UHPFRC at different ages follows a similar trend up to the first crack strength. The steel fiber content in UHPFRC appears to have a relatively small effect on the pre-cracking compressive strength and elastic modulus. Steel fibers in UHPFRC increase the modulus of elasticity and peak strength over that for UHPC by (6 to 9 %) and (15 to 19%), respectively. This is not a significant increase compared to the results reported for the tensile tests. However, steel fiber content was influential on the post-cracking behavior of UHPFRC compression tests; see Fig. 3 [2,9,11].

For the UHPC concrete, the elastic behavior was followed until the peak strength. The failure occurred with a sudden strain softening, similar to its tensile strength. Failure of the UHPC specimen occurred with the formation of the first crack when lateral deformation exceeded its tensile capacity. The UHPC specimens lost all their strength and failed in an abrupt, explosive manner, see Fig. 15. In contrast, the UHPFRC specimens behaved elastically to approximately 90–95 % of their compressive strength. At the end of the elastic stage, hairline cracks form, followed by strain hardening behavior (compression hardening) up to the peak strength. However, strain hardening behavior did not occur in some tests but failed after initial cracking. Following the peak strength, a progressive strain softening occurs in which the presence of steel fibers governs this stage, similar to its tensile behavior. The interaction between the fibers and the matrix contributed to the ductile compressive failure, where the concrete surface remained intact even after a total strength loss, see Fig. 3.

Furthermore, results obtained from this method for the modulus of elasticity of the UHPFRC at different ages were compared to conventional test methods using strain gauges [2,11]. Some of these fiber types

are very expensive, such as steel and carbon fibers. Generally, steel fibers are used for UHPFRC. The steel fibers differ in size, shape, and mechanical properties, as shown in Fig. 2 b.

1.3. Direct tensile strength and fracture energy

The direct tensile strength, also known as uniaxial tensile strength, represents concrete's true tensile properties. Normal concrete has a low tensile strength, typically between 2.1 and 4.8 MPa, with low ductility. However, the tensile strength of UHPFRC is reported to be in the range of 8 to 13.5 MPa, with better ductility properties. This improvement was reported to be highly dependent on the type, quantity, and orientation of steel fibers in the mix. Moreover, the fiber–matrix bond strength was reported to influence this parameter significantly [11]. The behavior and value of the tensile strength of UHPFRC are considerably enhanced compared to normal concrete. Therefore, studying this concrete's tensile strength and ductility is vital due to its contribution to tensile resistance in structural applications, particularly highway bridge applications (Fig. 4 (a)). Uniaxial tensile tests need to be performed to obtain the direct tensile strength and the tensile stress–strain relationship for UHPFRC. However, this test is avoided due to many implications involved during the test, in particular, for fiber-reinforced concrete. In addition, many research studies have attempted to design suitable test methods for fiber reinforced concrete, each with its interpretation [2,11]. The reliability of the test methods reported in the literature is questionable due to the variation of the results reported. Flexural toughness is similar to fracture energy and is an important material property of concrete to measure ductility. It relates to the ability of concrete to absorb energy after the formation of the first crack. Flexural toughness for a typical UHPFRC mix with and without fibers was approximately 120 and 0.99 J [11]. The inclusion of fibers in UHPFRC and bond strength was reported to benefit this parameter significantly. However, increasing the fiber content to a very high percentage, i.e., 6 %, might have an adverse effect and result in fiber balling which can reduce the workability. This was demonstrated experimentally, where the ideal percentage was reported to be 2 to 3.5 %, and the fracture energy of UHPFRC ranged between 19,000 to 24,000 J/m² (Fig. 4 (b)).

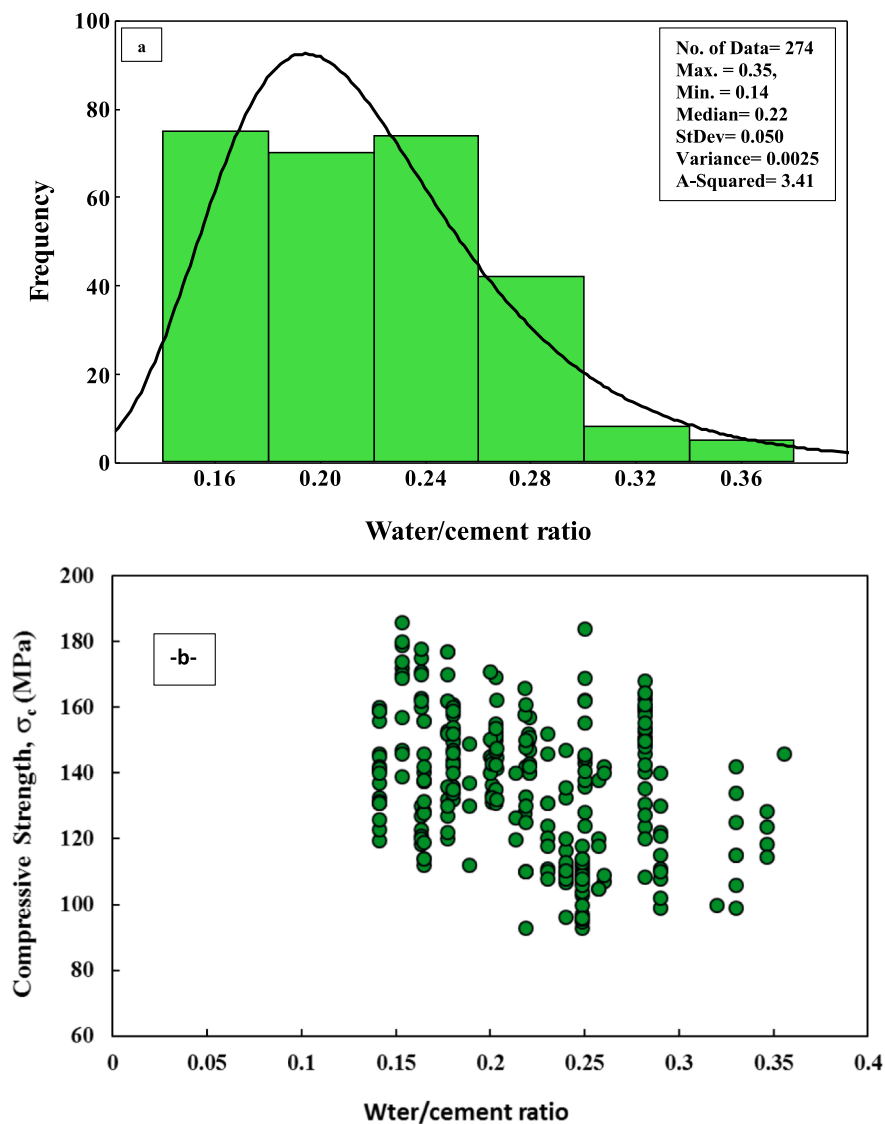


Fig. 5. (a) Histogram for w/c used to prepare the UHPFRC mix and (b) Relationship between w/c and compressive strength of UHPFRC.

2. Methodology

The collected data from various literature for this paper was 274 datasets inserting all data into an excel sheet; the data were sorted, statistically assessed, divided, and separated into three groups. The largest group, which consisted of two-thirds of the data, was named the training data set and utilized to develop the models. The other two groups, each with one- to six of the data set, were used for testing and validating the proposed models. Table 1 includes the detailed ranges and information about each variable studied in the study, which includes (a) SF content, (b) cement content, (c) w/c, (d) curing temperature, (e) SP content, (f) sand, (g) curing time, (h) fiber content, (i) fiber AR, (j) Water content, and (k) SP content with compressive strength of the UHPFRC. All mentioned independent parameters were utilized to quantify and estimate the compressive strength and compare the results with the measured strength. The current study's process is simply depicted in Fig. 1.

- Step 1: Data were collected from different research studies.
- Step 2: Statistical analyses were performed on the input variables.
- Step 3: Splitting the data randomly into three parts (training, testing, and validation).
- Step 4: Four soft computing techniques were performed on the

training data set.

Step 5: Different performance criteria were used to compare the developed models.

Step 6: Sensitivity analyses were conducted to find the most effective parameter for the compressive strength of UHPFRC.

3. Statistical evaluation

This part of the paper is all about the statistical analysis of the dependent and independent variables separately to determine whether a strong relationship exists between each variable and the compressive strength of UHPFRC. Thus, the plot of all considered parameters, including (a) SF content, (b) cement content, (c) w/c, (d) curing temperature, (e) SP content, (f) sand, (g) curing time, (h) fiber content, (i) fiber AR, (j) water content, and (k) SP content with compressive strength was drawn (Fig. 5, Fig. 6, and Fig. 7), also to clarify the distribution of every variable with the compressive strength, statistical functions such as Standard Deviation (SD), Variance, Skewness, and Kurtosis were calculated.

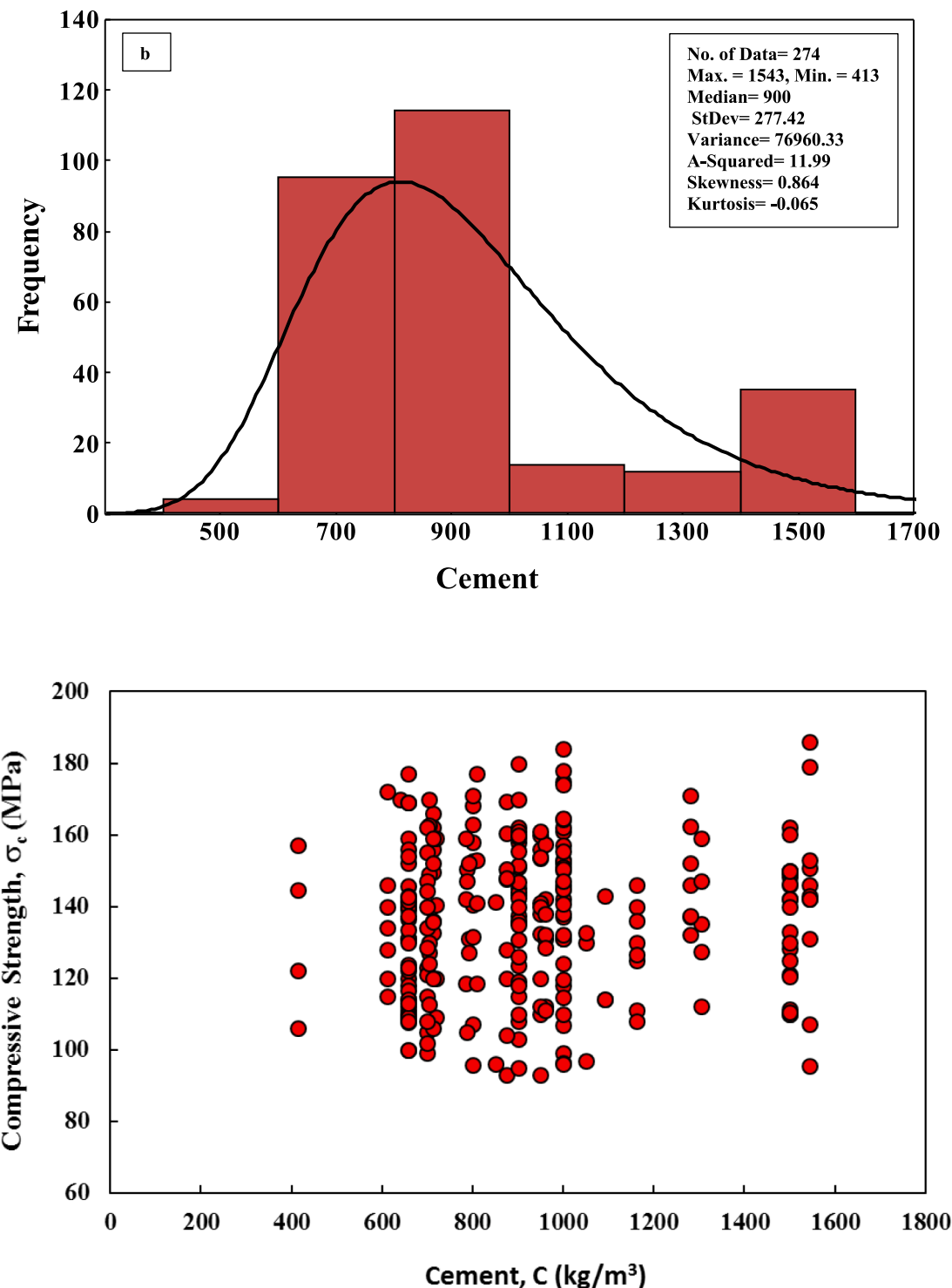


Fig. 6. (a) Histogram for cement content used to prepare the UHPFRC mix and (b) Relationship between cement content and compressive strength of UHPFRC.

3.1. Compressive strength

According to the total collected data, the σ_c of UHPFRC mixtures ranged between 90 and 186 MPa, with a median of 138.5 MPa. From the statistical analysis, the values for other variables were as follows: variance of 435.37, A-squared of 1.83, the standard deviation of 20.87, and value of skewness and kurtosis were -0.106 and -0.745, respectively.

4. Modeling

According to the correlation matrix, no direct relationship was obtained from the analyzed data results in section 3; no direct relationship was obtained according to the correlation matrix (Fig. 8). Therefore, to quantify the influence of each parameter on the σ_c of UHPFRC.

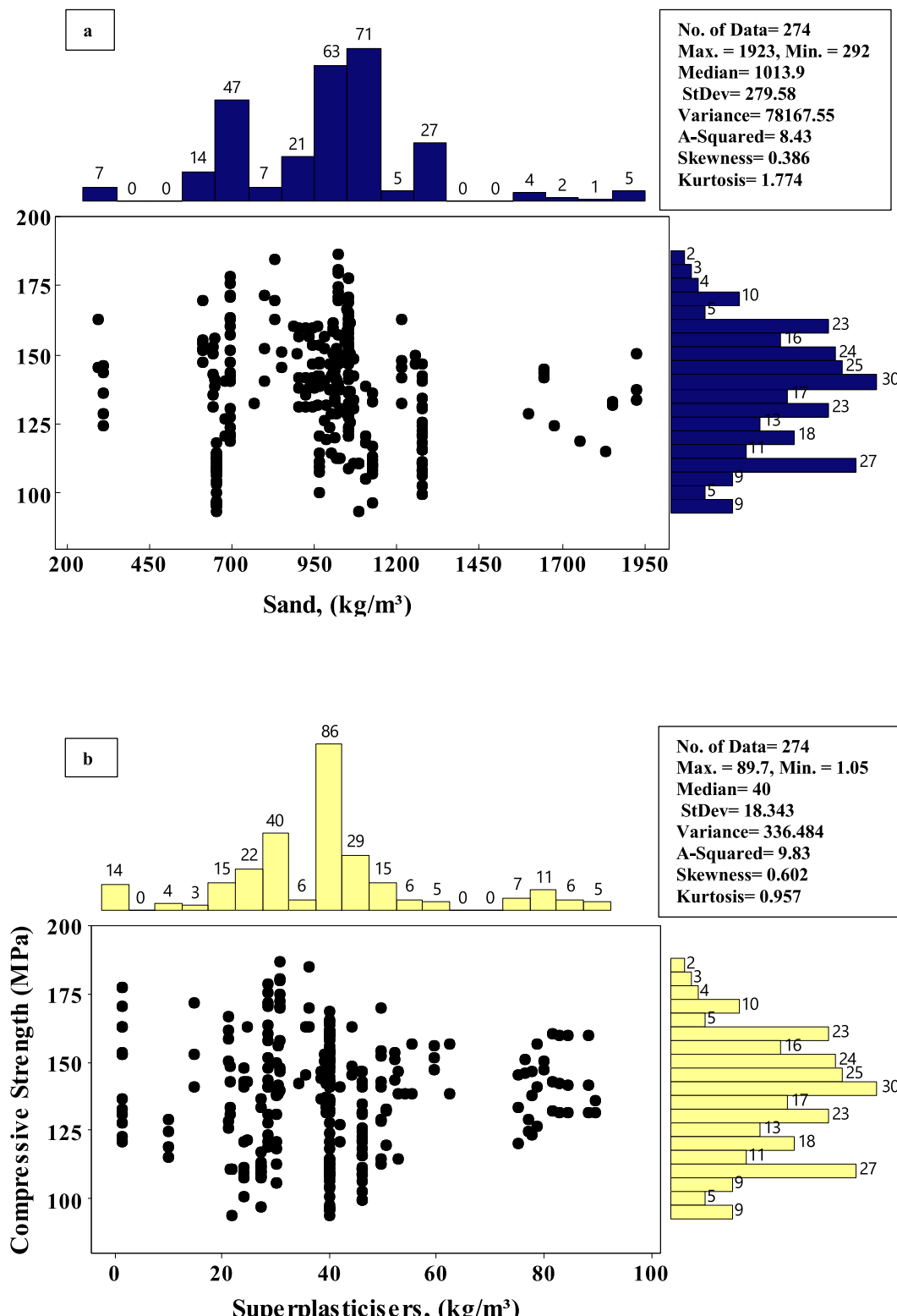


Fig. 7. Histogram for (a) w/c, (b) cement, (a) sand, (b) SP, (c) SF, (d) Curing temperature, (e) Curing age, (f) Fiber content, and (g) fiber aspect ratio of UHPFRC mixtures.

4.1. Nonlinear relationship model (NLR)

This study focuses on designing a model that evaluates the effect of the maximum number of parameters on the σ_c of UHPFRC. Nonlinear regression is a general method for evaluating the compressive strength used in this study [39]. But to increase the reliability of the predicted

strength value Eq. (1), eleven variables were proposed.

$$\begin{aligned} \sigma_c = & a + b^* \left(\frac{w}{c} \right)^c + d^*(C)^c + f^*(W)^g + h^*(S)^i + j^*(SP)^k + l^*(SF)^m + n^*(t)^o \\ & + i^*(Fb)^p + q^*(AR)^r + z^*(T)^w + x^*(FC)^y \end{aligned} \quad (1)$$

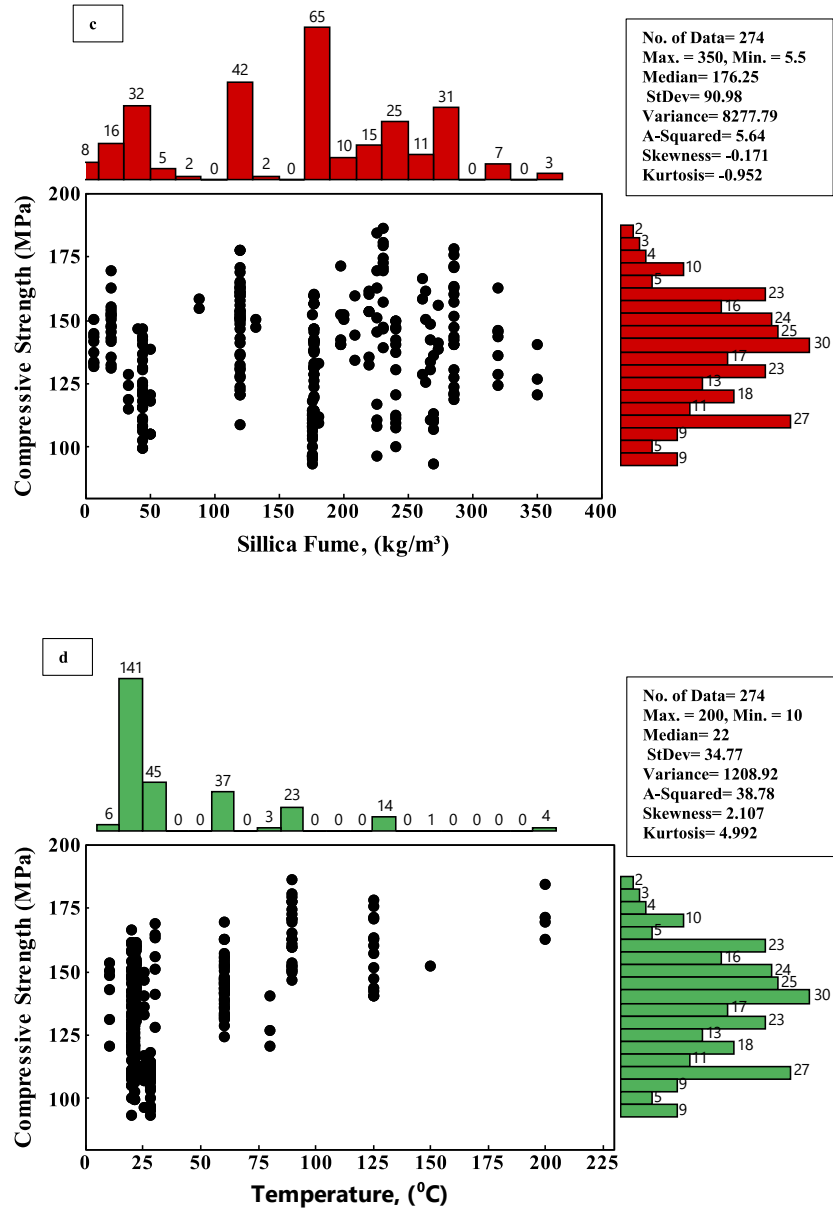


Fig. 7. (continued).

Where a to y are model parameters.

Where β_0 to β_{22} are the model parameters and were obtained by using the Least Square Method.

4.2. Pure quadratic model

Pure Quadratic technique (model) (Eq. (2)) was used to evaluate the σ_c of UHPFRC as follows:

4.3. M5P tree model

M5P-tree is a modified version of the Quinlan M5 technique [56–58]. One of the key benefits of tree modeling is its capability to efficiently manage massive volumes of data with an infinite number of attributes

$$\begin{aligned} \sigma_c = & \beta_0 + \beta_1 * \left(\frac{w}{c} \right) + \beta_2 * (C) + \beta_3 * (W) + \beta_4 * (S) + \beta_5 * (SP) + \beta_6 * (SF) + \beta_7 * (t) + \beta_8 * (Fb) + \beta_9 * (AR) + \beta_{10} * (T) + \beta_{11} * (FC) + \beta_{12} * \left(\frac{w^2}{c} \right) + \beta_{13} * (C^2) \\ & + \beta_{14} * (W^2) + \beta_{15} * (S^2) + \beta_{16} * (SP^2) + \beta_{17} * (SF^2) + \beta_{18} * (t^2) + \beta_{19} * (Fb^2) + \beta_{20} * (AR^2) + \beta_{21} * (T^2) + \beta_{22} * (FC^2) \end{aligned} \quad (2)$$

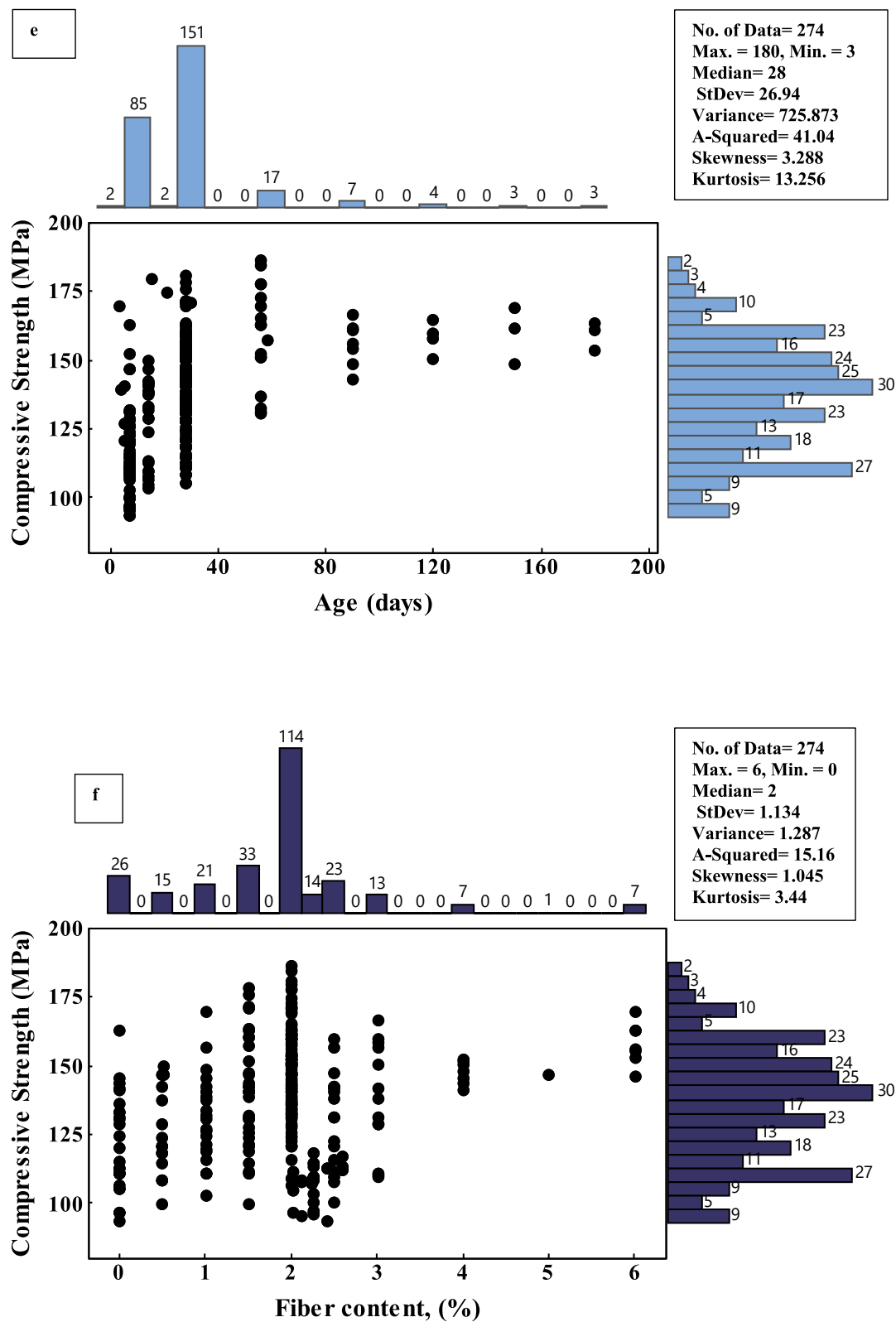


Fig. 7. (continued).

and dimensions.

Error estimates and details on the tree division criteria used in the M5P-tree model are displayed on each node. Any function associated with that node is evaluated using the feature that most reduces expected error. The M5P-tree model's tree division criteria are derived from node-level error estimations. The M5P-tree error represents the standard

deviation of a node's class value. The feature that minimizes the expected error reduction after analyzing each attribute at that node is used to divide the nodes. The data for child nodes (subtree or smaller nodes) has a lower standard deviation SD due to the branching approach. After evaluating all alternative structures, nodes that serve as parents (larger nodes) choose the structure with the best chance of reducing errors. This

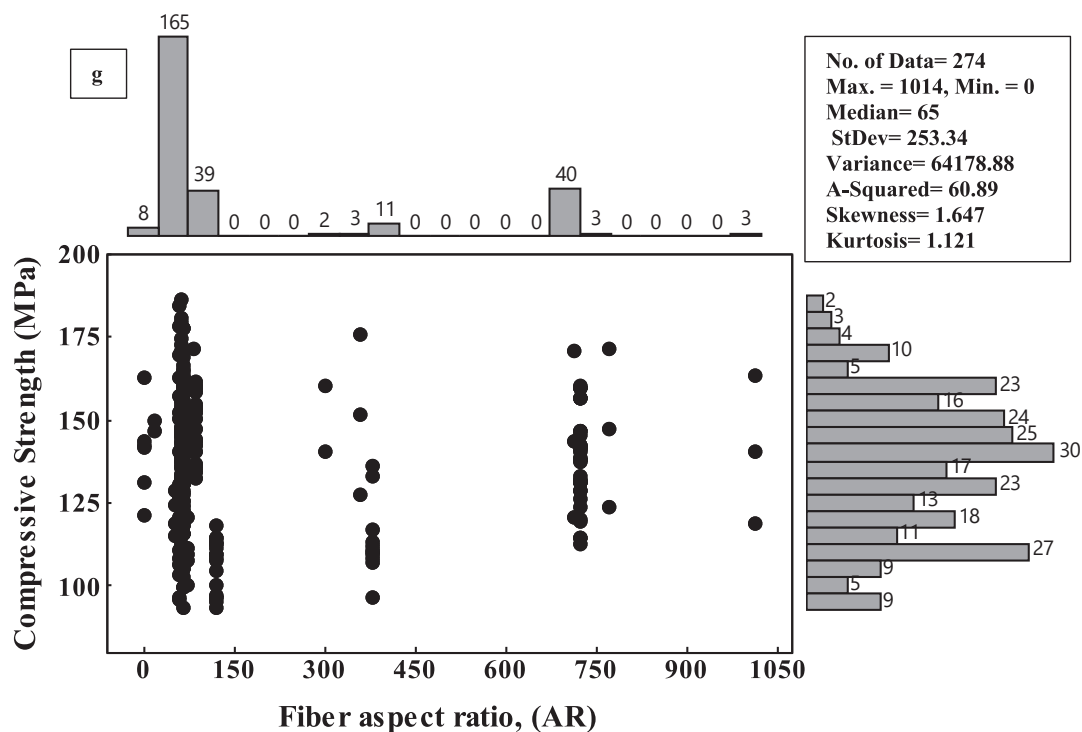


Fig. 7. (continued).

	w/c	C	W	S	SP	SF	t	F	AR	T	FC	σ_e
w/c	1.00	-0.18	0.41	0.17	-0.24	-0.30	0.21	0.27	-0.51	-0.12	0.10	-0.34
C	-0.18	1.00	0.81	-0.51	0.35	0.00	-0.28	0.22	0.07	-0.01	0.24	-0.25
W	0.41	0.81	1.00	-0.41	0.12	-0.10	-0.13	0.37	-0.28	-0.05	0.28	-0.43
S	0.17	-0.51	-0.41	1.00	-0.13	-0.55	0.06	-0.16	-0.13	-0.22	-0.24	-0.05
SP	-0.24	0.35	0.12	-0.13	1.00	-0.14	-0.13	-0.17	0.43	-0.23	-0.03	-0.01
SF	-0.30	0.00	-0.10	-0.55	-0.14	1.00	-0.10	-0.17	0.24	0.19	-0.07	0.08
t	0.21	-0.28	-0.13	0.06	-0.13	-0.10	1.00	0.11	-0.20	0.05	0.05	0.45
F	0.27	0.22	0.37	-0.16	-0.17	-0.17	0.11	1.00	-0.46	0.04	0.91	0.22
AR	-0.51	0.07	-0.28	-0.13	0.43	0.24	-0.20	-0.46	1.00	-0.07	-0.16	0.00
T	-0.12	-0.01	-0.05	-0.22	-0.23	0.19	0.05	0.04	-0.07	1.00	0.06	0.52
FC	0.10	0.24	0.28	-0.24	-0.03	-0.07	0.05	0.91	-0.16	0.06	1.00	0.26
σ_e	-0.34	-0.25	-0.43	-0.05	-0.01	0.08	0.45	0.22	0.00	0.52	0.26	1.00

Fig. 8. Correlation matrix for the properties of UHPFRC.

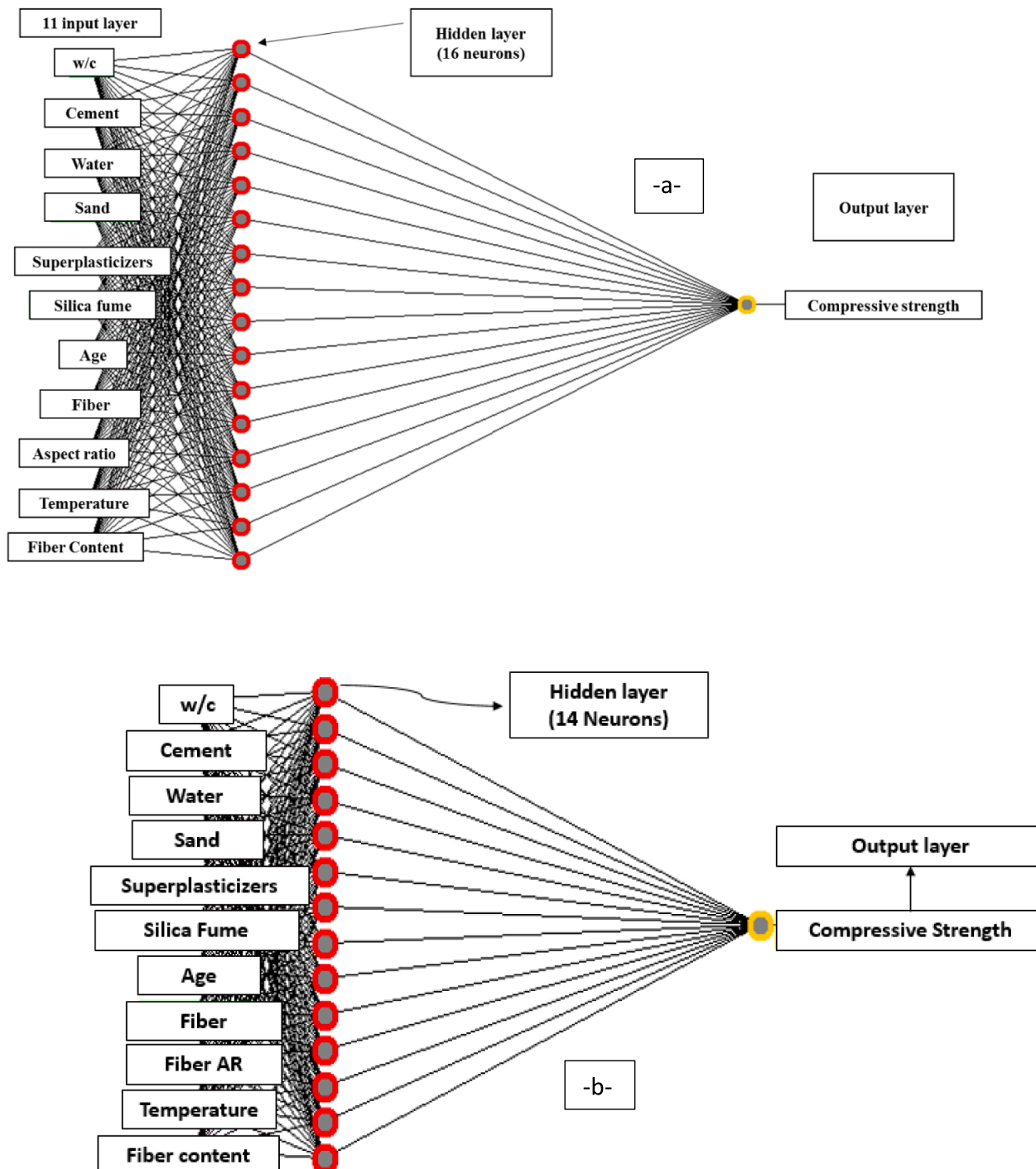


Fig. 9. Optimal neural network model structure (a) 16 neurons, and (b) 14 neurons.

division is also in charge of generating a massive tree-like structure that encourages overfitting.

4.4. Artificial intelligence (ANN)

The inverse of forwarding neural networks is ANNs [57–59]. As shown in Fig. 9, it comprises three separate layers: input, output, and hidden. The input layer receives the signal to be inspected. The output

layer is responsible for performing essential tasks such as prediction and classification. True computational ANN engines have many hidden layers between the input and output levels. Data travels from the source to the destination layer, similar to the feed-forward network in the ANN. Over trial cycles, the multi-hidden layer result was improved to determine the best number of hidden layers for a model in error reduction and R^2 . Due to the complexity of the Equation for several hidden layers, a single hidden layer consisting of sixteen neural networks was chosen for

Table 2
Properties of normal strength concrete collected from the literature.

References	Water/cement ratio	Curing time, t (days)	Compressive strength, σ_c (MPa)
[39]	0.43	7 and 28	35–43
[40]	0.49–0.66	28	31–51
[41]	0.45–0.90	28 and 90	20–46
[42]	0.32–0.42	28	38–46
[43]	0.6	28 and 90	23–48
[44]	0.5–0.8	28	19–43
[45]	0.53	7, 14, 28 and 90	27–39
[46]	0.53	1, 3, 7, 28 and 90	19–45
[47]	0.4	7, 28 and 90	27–43
[48]	0.49	7 and 28	24–33
[49]	0.5	7, 28, 56 and 90	34–47
[50]	0.36	7 and 28	25–39
[51]	0.43	7 and 28	34–46
[52]	0.5	28 and 56	17–30
[53]	0.4–0.5	3, 7, 14 and 28	15–50
[54]	0.33	7, 14 and 28	35–55
[55]	0.35–0.45	Up to 90	11–33
Ranged between	0.32–0.9	Up to 90 days	11–55

this study by trial and error to get better performance based on statistical measures such as RMSE, MAE (mean absolute error), and R^2 . The lower value of RMSE and MAE and the higher value of R^2 indicates that the model has good performance (Fig. 9). An ANN equation with a single hidden layer is depicted in Eqs. (3) and (4).

$$\beta_n = a_n(w/c) + b_n(C) + c_n(W) + d_n(S) + e_n(SP) + f_n(SF) + g_n(t) + h_n(F) + i_n(AR) + j_n(FC) + h_n(FC) + i_n \quad (3)$$

$$\sigma_c = \frac{\text{Node}_1}{1 + e^{-\alpha_1}} + \frac{\text{Node}_2}{1 + e^{-\alpha_2}} + \dots + \frac{\text{Node}_n}{1 + e^{-\alpha_n}} + \text{Threshold} \quad (4)$$

5. Assessment criteria for the developed models

The coefficient of determination (R^2), Root Mean Squared Error (RMSE), Mean Absolute Error (MAE), Scatter Index (SI), and OBJ were used to evaluate the precision and efficiency of the model predictions. Four other models were predicted. All models were assessed using several standard evaluation criteria to compare all models and select the most accurate one, such as; Model validation, lowest residual error, highest R^2 , lower MAE, OBJ, RMSI, and SI values.

Their equations are:

$$R^2 = \left[\frac{\sum_{i=1}^n (y_i - \bar{y})(x_i - \bar{x})}{\sqrt{\left[\sum_{i=1}^n (y_i - \bar{y})^2 \right] \left[\sum_{i=1}^n (x_i - \bar{x})^2 \right]}} \right]^2 \quad (5)$$

$$\text{RMSE} = \sqrt{\frac{\sum_{i=1}^n (y_i - x_i)^2}{n}} \quad (6)$$

$$\text{SI} = \frac{\text{RMSE}}{y_i} \quad (7)$$

y_i = experimental value; x_i = predicted value by the proposed model; \bar{y} = the average value of experimental values; \bar{x} = average of the predicted value, and n is the number of data points.

6. Analysis and output

The relationship between measured and predicted values of compressive strength for UHPFRC using four models was compared with

100 data of normal strength concrete with the strength range of 11 to 55 MPa (Table 2) collected from different research studies [39–55], as shown in Fig. 10a, 11a, 12a, 13a.

6.1. Nonlinear relationship model (NLR)

The connection between measured and predicted σ_c of UHPFRC for training, validating, and testing is shown in Fig. 10a. The value of each parameter in the existing model was calculated by optimizing the sum of error squares and the least square method Eq. 8. represent the final result of NLR.

$$\begin{aligned} \sigma_c = & -2092 + 1131 * \left(\frac{W}{C} \right)^{-0.04} + 1438 * (C)^{-0.02} + 1.97 * (W)^{-3.86} + 317 * (S)^{-0.03} \\ & + 14.9 * (SP)^{0.16} - 1251 * (SF)^{0.0008} + 743 * (t)^{0.017} + 0.21 * (Fb)^{0.84} \\ & - 0.03 * (AR)^{0.006} - 0.009 * (T)^{-0.014} + 0.005 * (FC)^{0.094} \end{aligned} \quad (8)$$

The predicted compressive strength ranged between 0.82 and 1.21 MPa (Fig. 10 b). Based on the above Equation, the water to cement ratio has highly impacted the σ_c of UHPFRC, and the aspect ratio has the least. The value for assessment parameters such as R^2 , RMSE, and MAE is 0.70, 11.55 MPa, and 8.719 MPa.

6.2. Pure quadratic model

In Fig. 11a, the predicted σ_c is compared to the measured σ_c produced from UHPFRC's training, testing, and validation datasets. As demonstrated in Fig. 11b, the residual error ranged from 0.83 to 1.15. According to this model, the w/c ratio and Fiber content concentration are the most important factors impacting the compressive strength of UHPFRC. The Pure Quadratic model with distinct variable parameters (Equation (9)) can be represented as follows:

$$\begin{aligned} \sigma_c = & 35 + 141.4 * \left(\frac{W}{C} \right) + 0.07 * (C) - 0.27 * (W) + 0.01 * (S) + 0.42 * (SP) \\ & + 0.14 * (SF) + 0.67 * (t) + 0.12 * (Fb) - 0.02 * (AR) + 0.48 * (T) \\ & - 1.87 * (FC) + 0.014 * \left(\frac{W^2}{C} \right) - 1.5 * 10^{-5} * (C^2) - 0.0002 * (W^2) \\ & - 4.85 * 10^{16} * (S^2) - 0.002 * (SP^2) - 0.003 * (SF^2) - 0.0026 * (t^2) \\ & - 0.0014 * (Fb^2) - 1.8 * 10^{-5} * (AR^2) - 0.001 * (T^2) + 0.52 * (FC^2) \end{aligned} \quad (9)$$

This model's R^2 , RMSE, and MAE parameters are 0.83, 8.50, and 6.89 MPa.

6.3. M5P tree model

The M5P tree model (with value m) was developed [60–64]. In this work, the M5P-tree model tree is utilized to forecast the compressive strength of conventional concrete using 274 mix-design data. As noted before, 2/3 of the dataset was randomly chosen for training and the remaining 1/6 for testing, and 1/6 for validation prediction [41–44]. The training, testing, and validation sets were examined using various predictive accuracy criteria. The R^2 , MAE, and RMSE were all employed to assess the suggested performance of the model in this research. The M5P-tree technique divides the input space (independent variables) into two linear tree regression functions (marked LM1 and LM2). $Y = b_0 + b_1 * X_1 + b_2 * X_2$, where b_0 , b_1 , and b_2 are linear regression constants representing the model parameters. The relation between predicted and measured compressive strength is shown in Fig. 12. The study dataset has a $\pm 15\%$ error line, indicating that all measured values fall within the $\pm 15\%$ error line. The coefficient of determination R^2 for this model is 0.82, which indicates that the model performance is better than the NLR model. The statistical evaluation parameters, such as R^2 and RMSE, 0.828 and 6.344 MPa, respectively (Fig. 12).

Age (days) ≤ 14 use LM1.

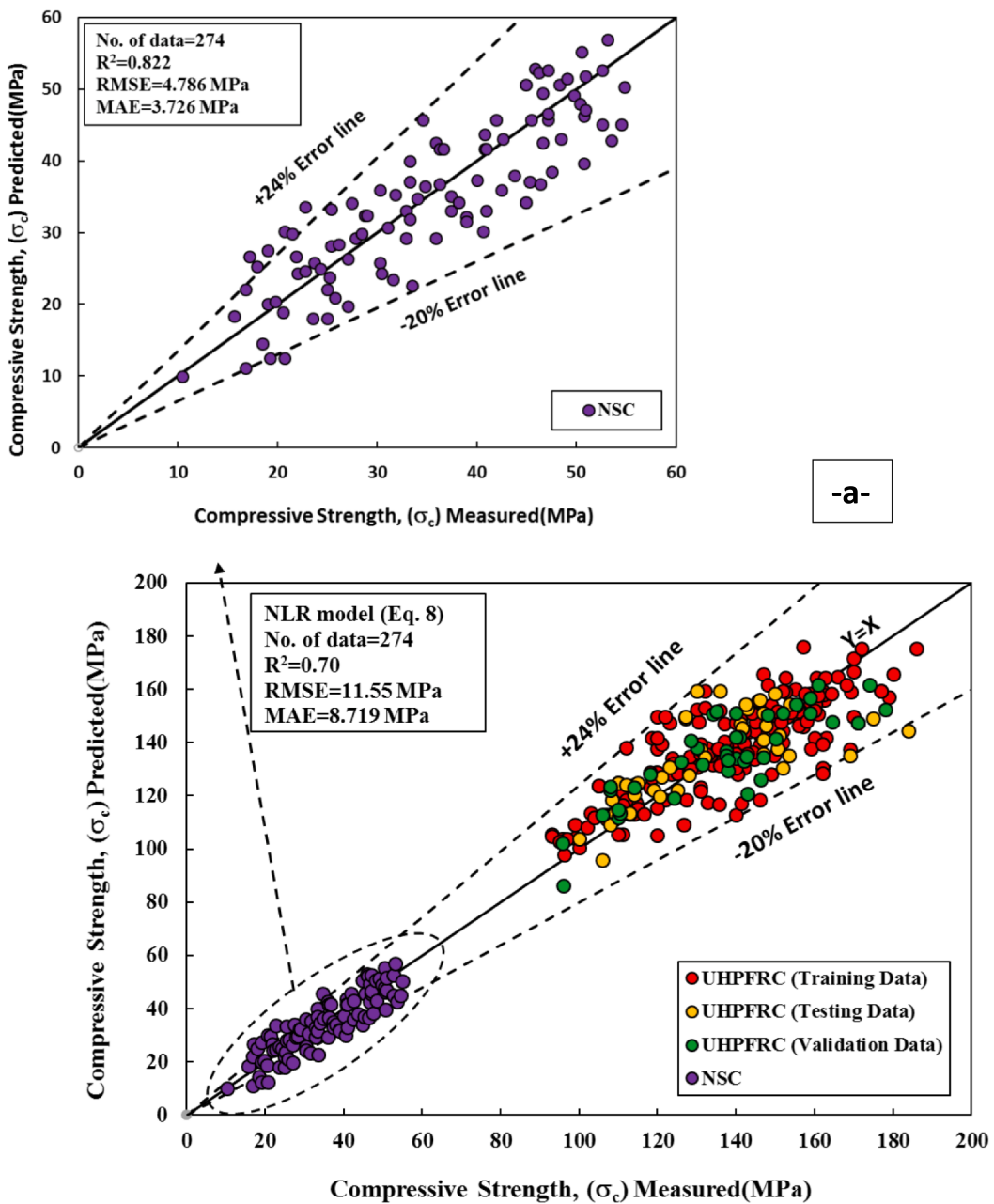


Fig.10. Comparison between measured and predicted the σ_c of UHPFRC using Non-Linear Regression Model (NLR) (a) datasets and (b) residual error.

Age (days) > 14 use LM2.

LM num: 1

$$\begin{aligned} \sigma_c = & 65.175 * w/c + 0.0063 * C - 0.1756 * W + 0.2007 * SP + 1.4205 * t \\ & + 0.1261 * F + 0.3807 * T + 118.8463 \end{aligned} \quad (10)$$

LM num: 2

$$\begin{aligned} \sigma_c = & 0.0219 * C - 0.2277 * W + 0.274 * SP + 0.0161 * SF + 0.2 * t \\ & + 0.0913 * F + 0.2342 * T + 124.1994 \end{aligned} \quad (11)$$

6.4. Artificial neural network (ANN)

The network was fed training, testing, and validation data to forecast the σ_c values for the appropriate input parameters (Fig. 9). The development of an ANN model is an iterative process (such as the number of hidden layer neurons, learning rate, momentum, and iteration). Nineteen neural networks were used in this study to represent hidden layers. The learning rate is 0.1, the training length is 50,000, and the momentum is 0.1. The number of epochs is also a hyperparameter that controls how many times the learning algorithm may process the

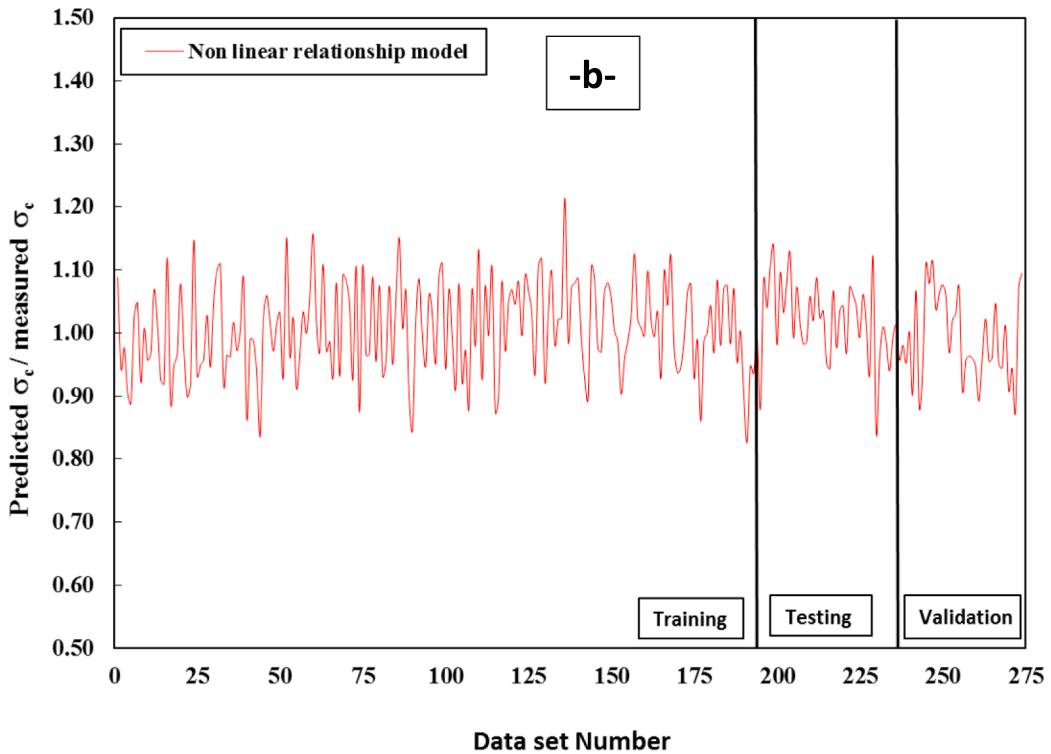


Fig.10. (continued).

training dataset. The greater the number of epochs, the higher the R^2 and the lower the RMSE as the error is minimized. The predicted versus actual values of σ_c are shown in Fig. 13. Choosing proper input variables is critical in system modeling [46]. The input variables picked should provide all necessary information about the goal values. Eleven distinct parameters were considered in this investigation to predict the σ_c of UHPFRC. Iterative development is required while creating an ANN model (such as the number of neurons, number of hidden layers, momentum, learning rate, and iteration). One hidden layer, including sixteen neural networks, was used in this study, with a learning rate of 0.1, a momentum of 0.1, and a training length of 50000.

Furthermore, the number of epochs is a hyperparameter that

specifies the number of times the learning algorithm may process the training dataset. The bigger the number of epochs, the higher the R^2 , the lower the RMSE, and the lower the MAE as the error is minimized. Based on statistical variables, the ANN model predicts the σ_c of UHPFRC more accurately than the NLR, M5P-tree, and pure quadratic models. ANN is a form of machine learning that employs a feed-forward algorithm with a high iteration rate to minimize the error percentage. R^2 , RMSE, and MAE (mean absolute error) parameters for this model are 0.977, 3.197 MPa, and 2.275 MPa, respectively. Additionally, the SI value for the

current model is 0.023 for the training dataset (Fig. 14).

$$\sigma_c = \frac{-3.67}{1 + e^{-\alpha 1}} + \frac{-3.18}{1 + e^{-\alpha 2}} + \frac{2.05}{1 + e^{-\alpha 3}} + \frac{2.10}{1 + e^{-\alpha 4}} + \frac{2.02}{1 + e^{-\alpha 5}} + \frac{-1.2}{1 + e^{-\alpha 6}} + \frac{-2.56}{1 + e^{-\alpha 7}} + \frac{-2.98}{1 + e^{-\alpha 8}} + \frac{-1.76}{1 + e^{-\alpha 9}} + \frac{-1.77}{1 + e^{-\alpha 10}} + \frac{2.68}{1 + e^{-\alpha 11}} + \frac{2.69}{1 + e^{-\alpha 12}} + \frac{2.30}{1 + e^{-\alpha 13}} + \frac{-2.42}{1 + e^{-\alpha 14}} + \frac{-2.59}{1 + e^{-\alpha 15}} + \frac{1.94}{1 + e^{-\alpha 16}} + 0.34 \quad (12)$$

$$\begin{bmatrix} -0.28 & -1.67 & -0.35 & 2.91 & 2.15 & 2.38 & 1.92 & 0.63 & 0.28 & -2.43 & 2.66 & -2.12 \\ 3.99 & 1.15 & 3.68 & 1.53 & 2.19 & 1.51 & -6.09 & 2.75 & 6.63 & 6.54 & 0.10 & 1.0 \\ 3.16 & -0.30 & 2.65 & -0.33 & -3.31 & 11.3 & 4.87 & 0.66 & 4.17 & -4.41 & -2.18 & 2.14 \\ 0.97 & 0.23 & 0.49 & 2.19 & 8.08 & 0.58 & -2.24 & 4.02 & 0.08 & -0.76 & 0.02 & -1.27 \\ 2.25 & -1.92 & -1.80 & 4.78 & -0.87 & 6.34 & 4.21 & -2.79 & 8.91 & -3.63 & 1.02 & -1.07 \\ 0.10 & 0.64 & 0.38 & 0.96 & 0.54 & 1.94 & 1.10 & -0.26 & 0.34 & 0.001 & -1.52 & -1.88 \\ 1.99 & 1.77 & 4.59 & 6.76 & 3.54 & 2.98 & -7.16 & 1.06 & 0.48 & -1.56 & -0.09 & -3.96 \\ 1.61 & 0.17 & 1.10 & 2.24 & 0.89 & 2.56 & 0.51 & 0.83 & -0.69 & 0.49 & 0.003 & -1.69 \\ -0.62 & 3.94 & -0.39 & 0.95 & 0.045 & -1.70 & 5.88 & -4.03 & -0.15 & -3.77 & -0.75 & -3.26 \\ 0.29 & 3.16 & 1.73 & -0.12 & -0.067 & -0.68 & 1.91 & -0.086 & -1.19 & 2.61 & -0.56 & -2.55 \\ -1.41 & 1.44 & 1.34 & 3.32 & 1.74 & -2.12 & -0.40 & -0.37 & -1.19 & 6.25 & -5.48 & -2.97 \\ -0.71 & 1.43 & -2.24 & 3.64 & 6.80 & 6.33 & -0.77 & 5.49 & 0.24 & 6.13 & 0.92 & 0.49 \\ 2.50 & 0.50 & 3.81 & -0.37 & -2.22 & 2.70 & -0.21 & -0.23 & 3.07 & 1.16 & -0.74 & -1.43 \\ 2.10 & -2.01 & -2.29 & -4.87 & -2.55 & 3.26 & -0.67 & -0.25 & 3.53 & -10.3 & -3.07 & -12.1 \\ 1.55 & -2.27 & -2.66 & -7.63 & 2.39 & 2.89 & -1.32 & 1.68 & 2.30 & 1.83 & 0.44 & -2.81 \\ -0.02 & -0.008 & -0.041 & -2.28 & -0.58 & 0.22 & 3.26 & 1.58 & -0.95 & -1.73 & -0.44 & -2.16 \end{bmatrix} \times \begin{bmatrix} w/c \\ C \\ t \\ SF \\ 1 \end{bmatrix} = \begin{bmatrix} \alpha_1 \\ \alpha_2 \\ \alpha_3 \\ \alpha_4 \\ \alpha_5 \\ S \\ \alpha_6 \\ SP \\ \alpha_7 \\ SF \\ \alpha_8 \\ t \\ \alpha_9 \\ F \\ AT \\ T \\ FC \\ \alpha_{13} \\ 1 \\ \alpha_{14} \\ \alpha_{14} \\ \alpha_{16} \end{bmatrix}$$

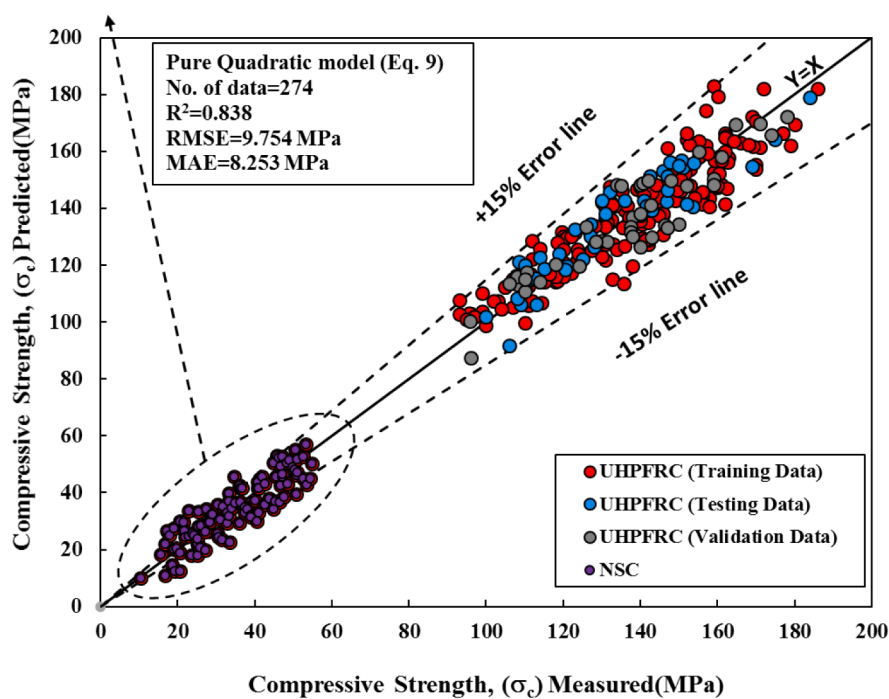
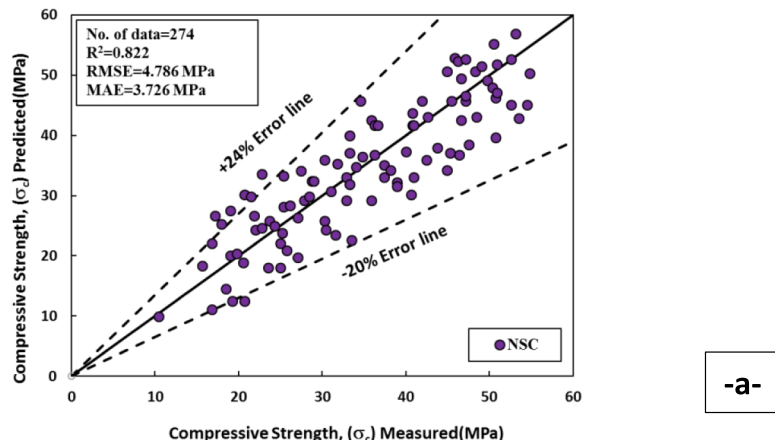


Fig. 11. Comparison between measured and predicted the σ_c of UHPFRC using Pure Quadratic Model (LR) (a) datasets and (b) residual error.

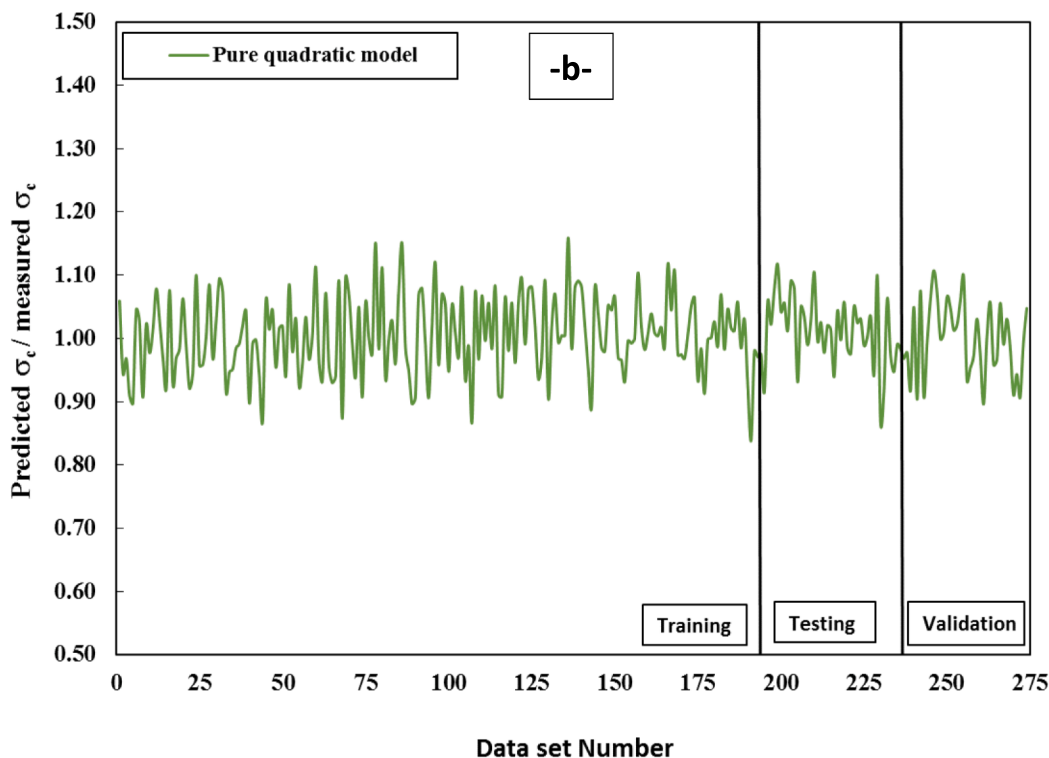


Fig. 11. (continued).

6.5. Comparison between developed models

Three statistical parameters (R^2 , MAE, RMSE) were utilized to examine the efficiency of the suggested novel models, as described in earlier sections. Compared to the NLR, Pure Quadratic, and M5P-tree models, the ANN model had the lowest RMSE and MAE and the highest R^2 values. Fig. 14 depicts the predicted σ_c vs the actual training and testing values for the all-developed model. The residual error for all models employing training, testing, and validating data sets is shown in Fig. 15, suggesting that the ANN model outperforms other models.

The SI assessment parameter values for the proposed models during the training, validating, and testing phases are shown in Fig. 16. The SI values for all models and stages (training, testing, and validating) were less than 0.1, suggesting good performance for all models, as shown in Fig. 16. Furthermore, like the other performance factors, the ANN model has lower SI values than other models. The ANN model had lower SI value values in all phases than the NLR model, including 208 percent lower in training, 68 percent lower in testing, and 50 percent lower in invalidating.

Finally, the M5P-tree model has a 3 percent higher SI value in the training phase and a 12.5 percent higher SI value in the validation phase, but a 60 percent lower SI value in the testing dataset than the pure quadratic model. This also demonstrated that the Pure quadratic model is more efficient and performs better when predicting the compressive strength of UHPFRC mixtures than the NLR and M5P tree models.

The box plot in Fig. 17 was also used to validate the model performance for conventional concrete's measured and predicted compressive strength. Between the first and third quartiles, a box plot is constructed. The line inside the box shows the median. The whiskers extend to the box minimum.

and maximum values from both ends. Thus, a box and whisker plot is a distribution graph; it depicts how data are distributed around the median, skewed, or symmetrical. The results indicated that the ANN model has a better performance than the other models.

6.6. Sensitivity investigation

A sensitivity test was performed on the models to determine and assess the most influencing variable that affects the σ_c of UHPFRC combinations [56]. The ANN model was used to analyze sensitivity, an efficient method. Several separate training data sets were employed in the sensitivity analysis, each with a single input variable extracted at a time. The assessment parameters for each training dataset, such as R^2 , RMSE, and MAE, were established individually. The data show that the most important and affecting variables for σ_c prediction of UHPFRC combinations are curing temperature, fiber content, and curing time. As a result, increasing the curing time and fiber content enhanced the σ_c significantly. The impact of mix proportions on the σ_c of UHPFRC is shown in Fig. 18. Based on the RMSE curing temperature and w/c parameters having the greatest and least impact on the output of the ANN model, respectively (Fig. 18), the same result was observed by [11].

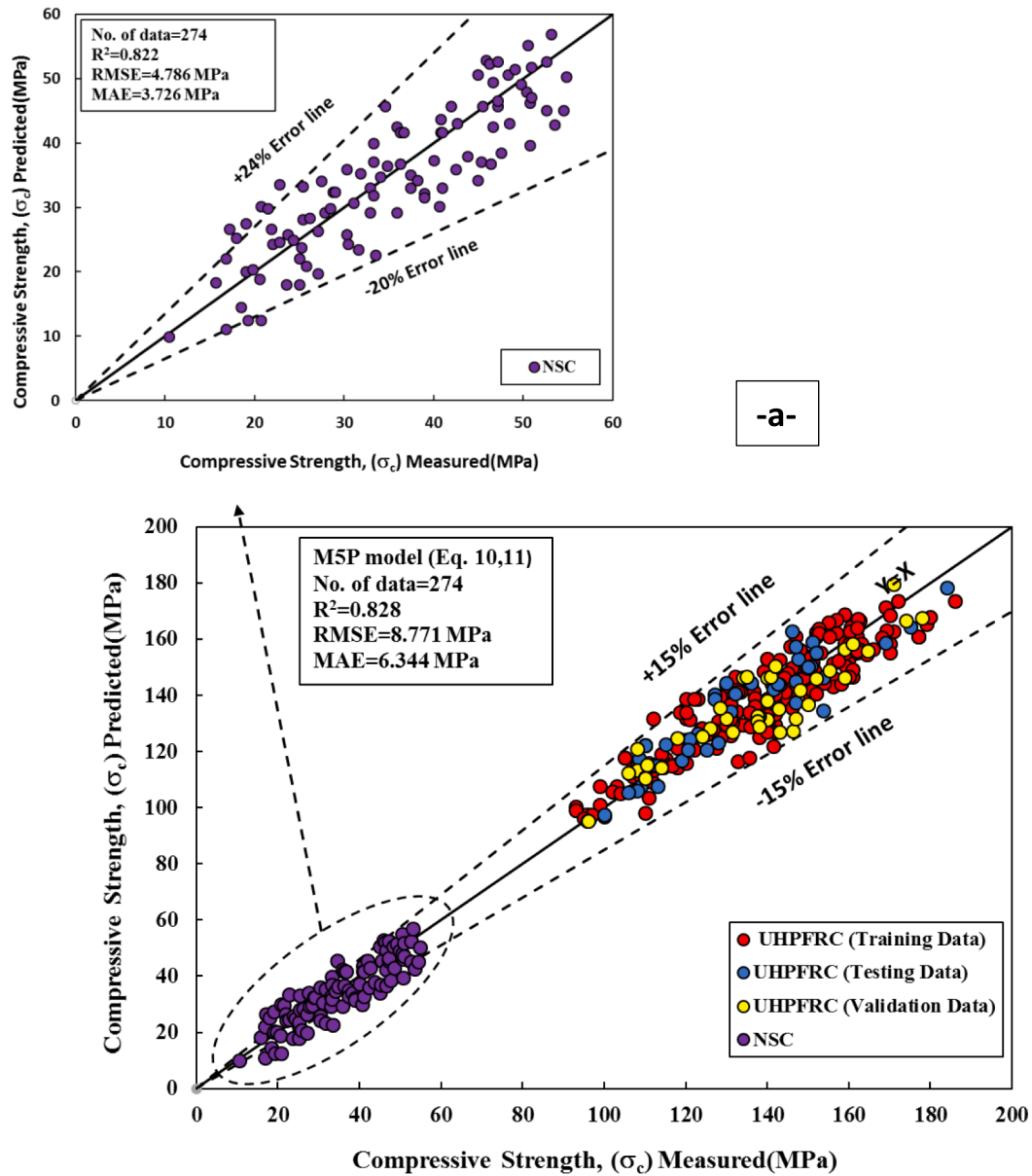


Fig. 12. Comparison between measured and predicted the σ_c of UHPFRC using M5P-tree Model (LR) (a) datasets and (b) residual error.

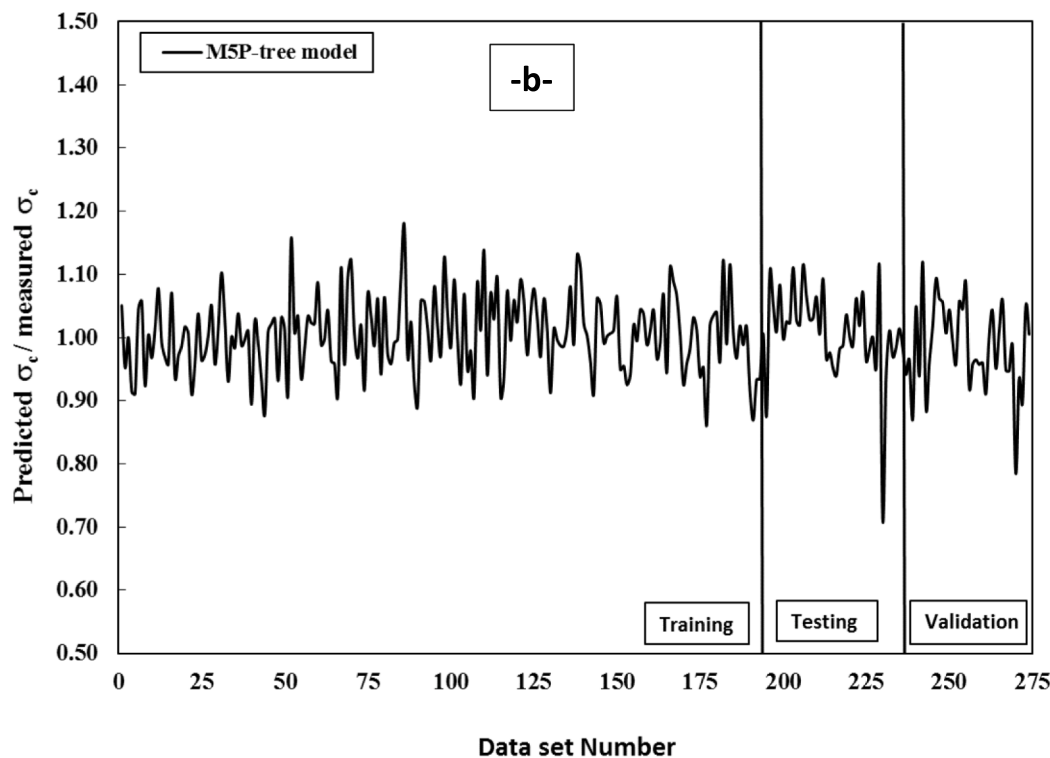


Fig. 12. (continued).

6.7. Limitation of this study

Although this study is based on a scientific study of various concrete elements, it has several flaws that must be addressed. The important limitations are defined below:

Machine learning models are a programming or scientific method where the training and testing of data are completed based on the capability of the models. While this investigation displays better accuracy, the compressive strength of UHPFRC may be predicted using the regression model by testing and training data. This study is completely fixated on models and gives a comprehensive compressive strength of UHPFRC prediction. However, for highly accurate, valuation-based collection of compressive strength data is very suitable for predicting the compressive strength. However, estimating the compressive strength of UHPFRC and traditional methods is not a high cost but a very time-consuming process compared to soft computing and machine learning models.

7. Conclusions

Models for compressive strength prediction that are precise and accurate will save time and money. The following conclusions were drawn based on the study and simulation of data derived from prior research to predict the compressive strength of UHPFRC for 274 different mixed compositions:

1. At 28 days of curing, the average compressive strength of UHPFRC was 140.1 MPa. The development of compressive strength was enhanced as the curing temperature increased.
2. The compressive strength of UHPFRC was increased to 180 MPa after 7 days of curing, which is linearly proportional to a curing temperature range between 10 and 90 °C.
3. Depending on the statistical analysis, the median percentage of Fiber content for the production of UHPFRC was 2 %. Furthermore, the percentage of fiber inside all mixes ranged between 0 and 6 %, with 3 to 180 days of curing and sand content ranging between 292 to 1923 kg/m³.
4. Based on the correlation matrix, the direct relationship between the compressive strength of UHPFRC and the mix proportions was not observed.
5. NLR model, pure quadratic model, M5P-tree, and ANN model were developed to predict the compressive strength of UHPFRC mixtures. The ANN model outperformed other training, testing, and validating data sets, with higher R² values, lower RMSE, MAE, lower OBJ values, and SI values.
6. All SI values were less than 0.1 for all models and phases (training, testing, and validating), indicating exceptional performance. Furthermore, the ANN model has lower SI value values in all phases than the NLR model. For example, 208 percent lower in training, 68 percent lower in testing, and 50 percent lower in validate.
7. conventional test methods developed for normal concrete such as tensile splitting, flexural and compression tests were applied to

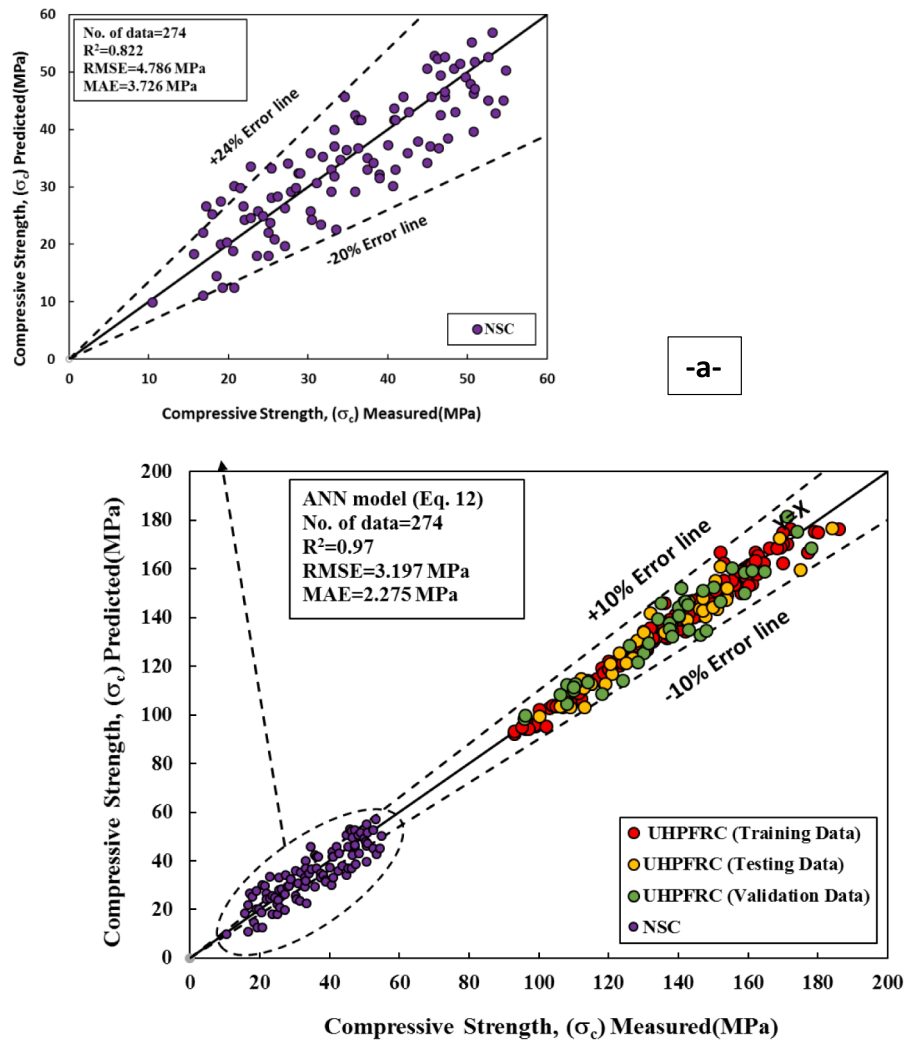


Fig. 13. Comparison between measured and predicted the σ_c of UHPFRC using ANN Model (LR) (a) datasets and (b) residual error.

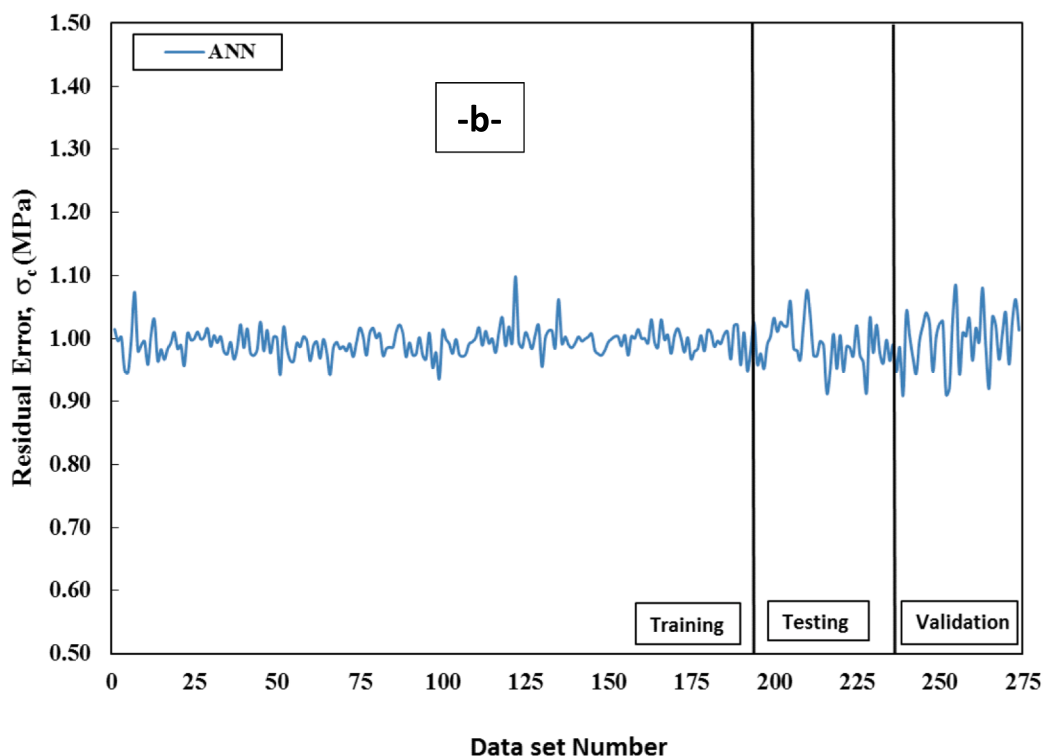


Fig. 13. (continued).

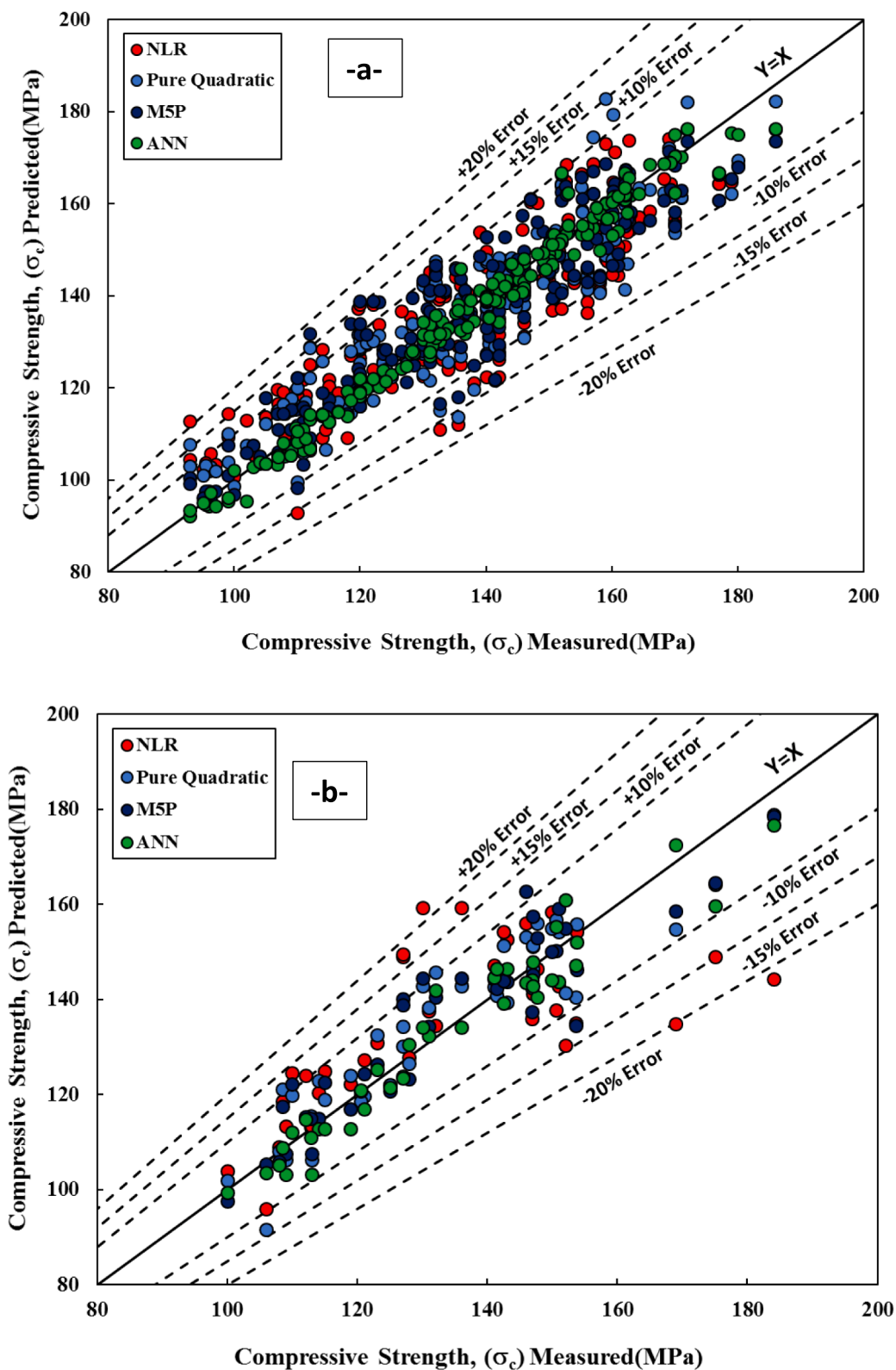


Fig. 14. Comparison between developed models of σ_c of UHPFRC using (a) training dataset, and (b) testing dataset.

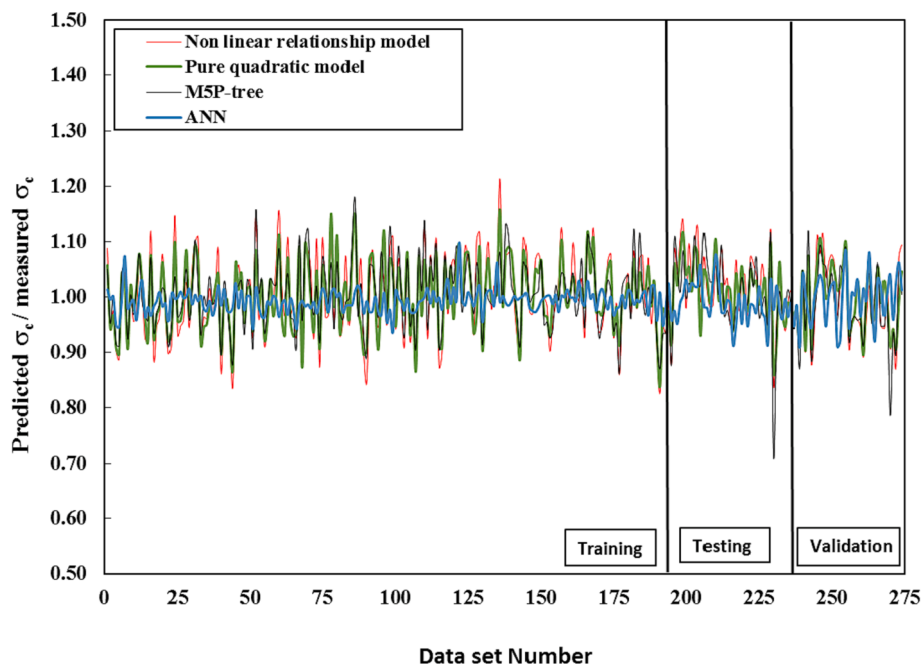


Fig. 15. Residual error of the compressive strength of UHPFRC using training, testing, and validating dataset.

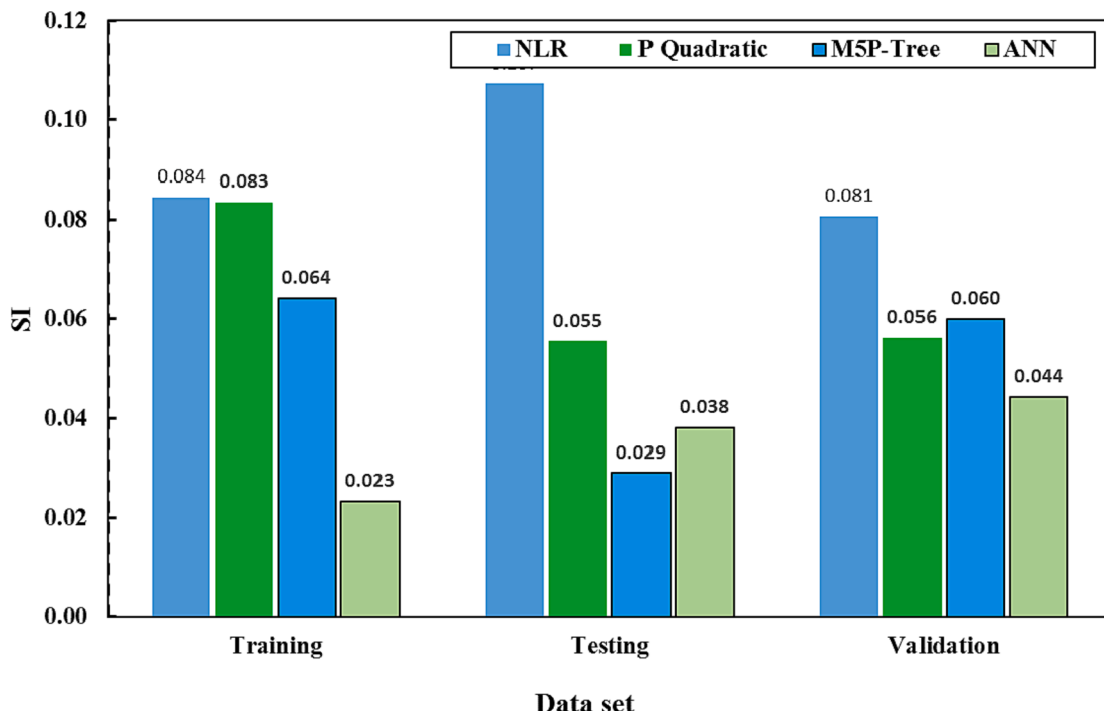


Fig. 16. Comparison of the SI performance parameter of different developed models for the training dataset and testing dataset.

define the stress-strain relationship of UHPFRC and UHPC in both tension and compression. The influence of steel fibre content and age on these properties was also studied. The existing test methods for normal concrete were found unreliable in determining the stress-strain relationship of UHPFRC in both tension and compression. In particular, for capturing the post-cracking behavior of the concrete. 8. The ANN model has the lowest RMSE values compared to other training, testing, and validation datasets. The proposed models' R^2 , RMSE, MAE, and boxplot functions indicated that the ANN model

had better centered mean square error and standard deviation performance.

- According to a sensitivity analysis, the curing temperature is the most critical input variable for forecasting the compressive strength of UHPFRC mixes.

Availability of data and materials.

The data supporting the conclusions of this article are included in the article.

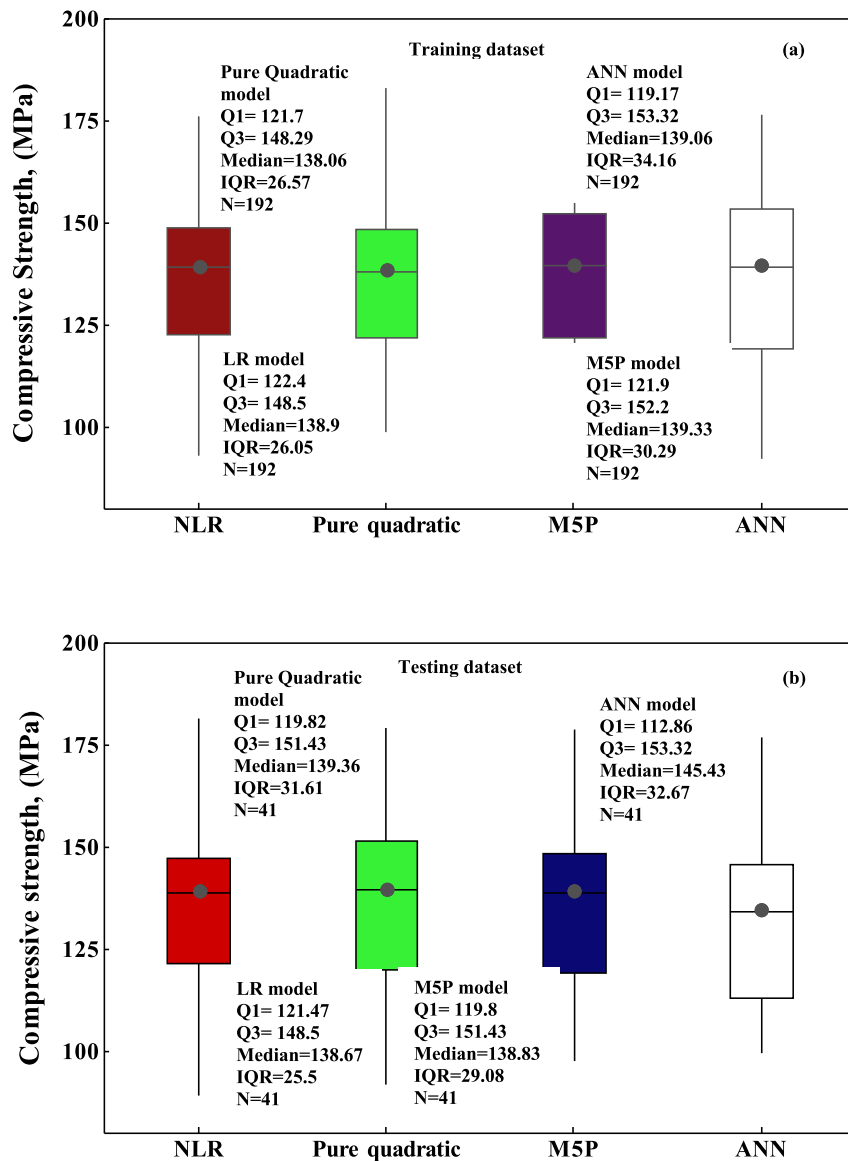


Fig. 17. Box Plot of predicted compressive strength of UHPFRC using different models (a) training dataset, and (b) testing dataset.

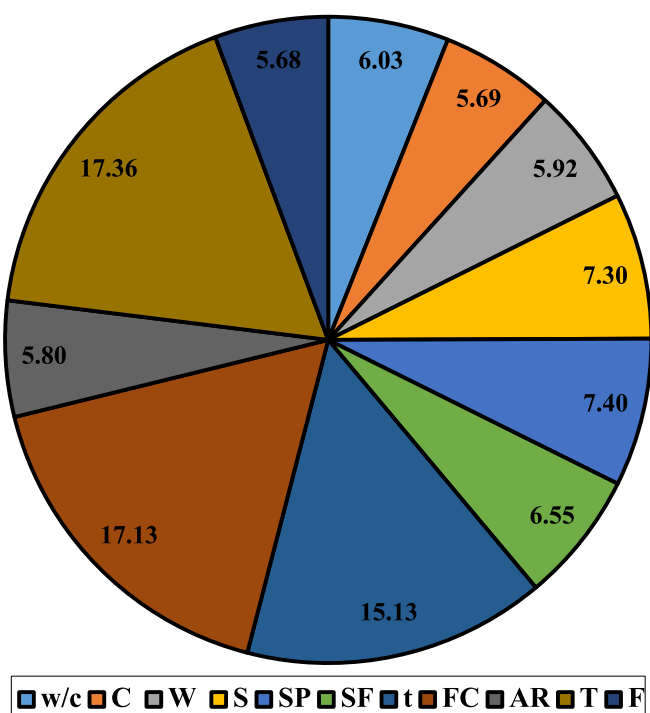


Fig. 18. Sensitivity analysis to investigate the effect of input variables on the σ_c based on RMSE by using the ANN model.

CRediT authorship contribution statement

Wael Emad: Conceptualization, Methodology. **Ahmed Salih Mohammed:** Conceptualization, Methodology. **Ana Bras:** Data curation, Writing – original draft. **Panagiotis G. Asteris:** Data curation, Writing – original draft. **Rawaz Kurda:** Data curation, Writing – original draft. **Zhyan Muhammed:** Data curation, Writing – original draft. **A.M. T. Hassan:** Supervision. **Shaker M.A. Qaidi:** Writing – review & editing. **Parveen Sihag:** Validation.

Declaration of Competing Interest

The authors declare that they have no known competing financial interests or personal relationships that could have appeared to influence the work reported in this paper.

References

- [1] P. Máca, R. Sovják, P. Konvalinka, Mix design of UHPFRC and its response to projectile impact, *Int. J. Impact Eng.* 63 (2014) 158–163, <https://doi.org/10.1016/j.ijimpeng.2013.08.003>.
- [2] A.M.T. Hassan, G.H. Mahmud, A.S. Mohammed, S.W. Jones, April). The influence of normal curing temperature on the compressive strength development and flexural tensile behaviour of UHPFRC with Vipulanandan model quantification, *In Structures* 30 (2021) 949–959, <https://doi.org/10.1016/j.istruc.2021.01.063>.
- [3] M.A. Mosaberpanah, O. Eren, Effect of Density on Compressive Strength of Ultra High Performance Fiber Reinforced Concrete (UHPFRC) Using Design of Experiment, in: Solid State Phenomena, Vol. 249, Trans Tech Publications Ltd., 2016, pp. 119–124, <https://doi.org/10.4028/www.scientific.net/SSP.249.119>.
- [4] A. Alsalman, C.N. Dang, G.S. Prinz, W.M. Hale, Evaluation of modulus of elasticity of ultra-high performance concrete, *Constr. Build. Mater.* 153 (2017) 918–928, <https://doi.org/10.1016/j.conbuildmat.2017.07.158>.
- [5] S.L. Yang, S.G. Millard, M.N. Soutsos, S.J. Barnett, T.T. Le, Influence of aggregate and curing regime on the mechanical properties of ultra-high performance fibre reinforced concrete (UHPFRC), *Constr. Build. Mater.* 23 (6) (2009) 2291–2298, <https://doi.org/10.1016/j.conbuildmat.2008.11.012>.
- [6] I.H. Yang, C. Joh, B.S. Kim, Structural behavior of ultra high performance concrete beams subjected to bending, *Eng. Struct.* 32 (11) (2010) 3478–3487, <https://doi.org/10.1016/j.engstruct.2010.07.017>.
- [7] D.Y. Yoo, H.O. Shin, J.M. Yang, Y.S. Yoon, Material and bond properties of ultra high performance fiber reinforced concrete with micro steel fibers, *Compos. B Eng.* 58 (2014) 122–133, <https://doi.org/10.1016/j.compositesb.2013.10.081>.
- [8] D.Y. Yoo, S.T. Kang, J.H. Lee, Y.S. Yoon, Effect of shrinkage reducing admixture on tensile and flexural behaviors of UHPFRC considering fiber distribution characteristics, *Cem. Concr. Res.* 54 (2013) 180–190, <https://doi.org/10.1016/j.cemconres.2013.09.006>.
- [9] G.H. Mahmud, Z. Yang, A.M. Hassan, Experimental and numerical studies of size effects of Ultra High Performance Steel Fibre Reinforced Concrete (UHPFRC) beams, *Constr. Build. Mater.* 48 (2013) 1027–1034, <https://doi.org/10.1016/j.conbuildmat.2013.07.061>.
- [10] V. Corinaldesi, G. Moriconi, Mechanical and thermal evaluation of ultra high performance fiber reinforced concretes for engineering applications, *Constr. Build. Mater.* 26 (1) (2012) 289–294, <https://doi.org/10.1016/j.conbuildmat.2011.06.023>.
- [11] A.M. Hassan, Ultra high performance fibre reinforced concrete for highway bridge applications, (Doctoral dissertation, University of Liverpool), 2013.
- [12] C. Magureanu, I. Sosa, C. Negruțiu, B. Heghes, Physical and mechanical properties of ultra high strength fiber reinforced cementitious composites, *Fracture Mechanics of Concrete and Concrete Structures*, Korea Concrete Institute, 2010, pp. 1497–11491.
- [13] A.A. Mala, A.F.H. Sherwani, K.H. Younis, R.H. Faraj, A. Mosavi, Mechanical and fracture parameters of ultra-high performance fiber reinforcement concrete cured via steam and water: Optimization of binder content, *Materials* 14 (8) (2021) 2016.
- [14] H.H. Qadir, R.H. Faraj, A.F.H. Sherwani, B.H. Mohammed, K.H. Younis, Mechanical properties and fracture parameters of ultra high performance steel fiber reinforced concrete composites made with extremely low water per binder ratios, *SN Applied Sciences* 2 (9) (2020) 1–12.
- [15] S. Kwon, T. Nishiwaki, T. Kikuta, H. Mihashi, Development of ultra-high-performance hybrid fiber-reinforced cement-based composites, *ACI Mater. J.* 111 (3) (2014) 309.
- [16] Z. Wu, C. Shi, W. He, L. Wu, Effects of steel fiber content and shape on mechanical properties of ultra high performance concrete, *Constr. Build. Mater.* 103 (2016) 8–14, <https://doi.org/10.1016/j.conbuildmat.2015.11.028>.
- [17] P.G. Asteris, A. Mamou, M. Hajihassani, M. Hasanipanah, M. Koopalipoor, T.T. Le, D.J. Armaghani, Soft computing based closed form equations correlating L and N-type Schmidt hammer rebound numbers of rocks, *Transp. Geotech.* 29 (2021), 100588.
- [18] E. Momeni, R. Nazir, D.J. Armaghani, H. Maizir, Prediction of pile bearing capacity using a hybrid genetic algorithm-based ANN, *Measurement* 57 (2014) 122–131.
- [19] M. Hasanipanah, M. Monjezi, A. Shahnazar, D.J. Armaghani, A. Farazmand, Feasibility of indirect determination of blast induced ground vibration based on support vector machine, *Measurement* 75 (2015) 289–297.
- [20] D.J. Armaghani, E.T. Mohamad, M.S. Narayanasamy, N. Narita, S. Yagiz, Development of hybrid intelligent models for predicting TBM penetration rate in hard rock condition, *Tunn. Undergr. Space Technol.* 63 (2017) 29–43.
- [21] H. Chen, P.G. Asteris, D. Jared Armaghani, B. Gordian, B.T. Pham, Assessing dynamic conditions of the retaining wall: developing two hybrid intelligent models, *Applied Sciences* 9 (6) (2019) 1042.
- [22] D.J. Armaghani, P.G. Asteris, A comparative study of ANN and ANFIS models for the prediction of cement-based mortar materials compressive strength, *Neural Comput. Appl.* 33 (9) (2021) 4501–4532.
- [23] M. Parsajoo, D.J. Armaghani, A.S. Mohammed, M. Khari, S. Jahandari, Tensile strength prediction of rock material using non-destructive tests: A comparative intelligent study, *Transp. Geotech.* 31 (2021), 100652.
- [24] B.T. Pham, M.D. Nguyen, T. Nguyen-Thoi, L.S. Ho, M. Koopalipoor, N.K. Quoc, H. Van Le, A novel approach for classification of soils based on laboratory tests using Adaboost, Tree and ANN modeling, *Transportation Geotechnics* 27 (2021), 100508.
- [25] P.A. Krahf, R. Carracedo, M.K. El Debs, Mechanical damage evolution in UHPFRC: experimental and numerical investigation, *Eng. Struct.* 170 (2018) 63–77, <https://doi.org/10.1016/j.engstruct.2018.05.064>.
- [26] A.M.T. Hassan, S.W. Jones, G.H. Mahmud, Experimental test methods to determine the uniaxial tensile and compressive behaviour of ultra high performance fibre reinforced concrete (UHPFRC), *Constr. Build. Mater.* 37 (2012) 874–882, <https://doi.org/10.1016/j.conbuildmat.2012.04.030>.
- [27] R. Yu, P. Spiesz, H.J.H. Brouwers, Mix design and properties assessment of ultra-high performance fibre reinforced concrete (UHPFRC), *Cem. Concr. Res.* 56 (2014) 29–39, <https://doi.org/10.1016/j.cemconres.2013.11.002>.
- [28] H. Jiang, A.S. Mohammed, R.A. Kazeroun, P. Sarir, Use of the Gene-Expression Programming Equation and FEM for the High-Strength CFST Columns, *Applied Sciences* 11 (21) (2021) 10468.
- [29] R. Aghayari, A.O. AL-Mwanes (2019). An Experimental Investigation of Mechanical Properties of The Ultra-High Performance Fiber Reinforced Concrete (UHPFRC).
- [30] L. Jin, R. Zhang, Y. Tian, G. Dou, X. Du, Experimental investigation on static and dynamic mechanical properties of steel fiber reinforced ultra-high-strength concretes, *Constr. Build. Mater.* 178 (2018) 102–111, <https://doi.org/10.1016/j.conbuildmat.2018.05.152>.
- [31] B.H. Mohammed, A.F.H. Sherwani, R.H. Faraj, H.H. Qadir, K.H. Younis, Mechanical properties and ductility behavior of ultra-high performance fiber reinforced concretes: Effect of low water-to-binder ratios and micro glass fibers, *Ain Shams Eng. J.* (2021), <https://doi.org/10.1016/j.asej.2020.11.008>.
- [32] A. Alsalman, C.N. Dang, J.R. Martí-Vargas, W.M. Hale, Mixture-proportioning of economical UHPC mixtures, *Journal of Building Engineering* 27 (2020), 100970, <https://doi.org/10.1016/j.jobe.2019.100970>.
- [33] P.R. Prem, B.H. Bharatkumar, N.R. Iyer, Influence of curing regimes on compressive strength of ultra high performance concrete, *Sadhana* 38 (6) (2013) 1421–1431.

- [35] R. Kurda, A. Salih, P. Shakor, P. Saleh, R. Alyousef, H. Ahmed, F. Aslanif, Mix design of concrete: Advanced particle packing model by developing and combining multiple frameworks, *Constr. Build. Mater.* 320 (2022), 126218.
- [36] A. Abdalla, A. Salih, Implementation of multi-expression programming (MEP), artificial neural network (ANN), and M5P-tree to forecast the compression strength cement-based mortar modified by calcium hydroxide at different mix proportions and curing ages, *Innovative Infrastructure Solutions* 7 (2) (2022) 1–15.
- [37] P.G. Asteris, M. Apostolopoulou, D.J. Armaghani, L. Cavalieri, A.T. Chountalas, D. Guney, M. Hajihassani, M. Hasanipanah, M. Khandelwal, C. Karamani, M. Koopialipoor, E. Kotsonis, T.-T. Le, P.B. Lourenço, H.-B. Ly, A. Moropoulos, H. Nguyen, B.T. Pham, P. Samui, J. Zhou, On the metaheuristic models for the prediction of cement-metakaolin mortars compressive strength, *Metaheuristic Computing and Applications* 1 (1) (2020) 63–99, <https://doi.org/10.12989/mca.2020.1.1.063>.
- [38] M. Parsajoo, D.J. Armaghani, P.G. Asteris, A precise neuro-fuzzy model enhanced by artificial bee colony techniques for assessment of rock brittleness index, *Neural Comput. & Appl.* (2021), <https://doi.org/10.1007/s00521-021-06600-8>.
- [39] S.A. Khedr, A.F. Idriss, Resistance of silica-fume concrete to corrosion-related damage, *J. Mater. Civ. Eng.* 7 (2) (1995) 102–107, [https://doi.org/10.1061/\(ASCE\)0899-1561\(1995\)7:2\(102\)](https://doi.org/10.1061/(ASCE)0899-1561(1995)7:2(102)).
- [40] M.G. Alexander, B.J. Magee, Durability performance of concrete containing condensed silica fume, *Cem. Concr. Res.* 29 (6) (1999) 917–922, [https://doi.org/10.1016/S0008-8846\(99\)00064-2](https://doi.org/10.1016/S0008-8846(99)00064-2).
- [41] M.F.M. Zain, M. Safiuddin, H. Mahmud, Development of high performance concrete using silica fume at relatively high water–binder ratios, *Cem. Concr. Res.* 30 (9) (2000) 1501–1505, [https://doi.org/10.1016/S0008-8846\(00\)00359-8](https://doi.org/10.1016/S0008-8846(00)00359-8).
- [42] N. Bouzoubaa, M.H. Zhang, V.M. Malhotra, Mechanical properties and durability of concrete made with high-volume fly ash blended cements using a coarse fly ash, *Cem. Concr. Res.* 31 (10) (2001) 1393–1402, [https://doi.org/10.1016/S0008-8846\(01\)00592-0](https://doi.org/10.1016/S0008-8846(01)00592-0).
- [43] A.D.N.A.N. Oner, S. Akyuz, R. Yildiz, An experimental study on strength development of concrete containing fly ash and optimum usage of fly ash in concrete, *Cem. Concr. Res.* 35 (6) (2005) 1165–1171, <https://doi.org/10.1016/j.cemconres.2004.09.031>.
- [44] J.M.R. Dotto, A.G. De Abreu, D.C.C. Dal Molin, I.L. Müller, Influence of silica fume addition on concretes physical properties and on corrosion behaviour of reinforcement bars, *Cem. Concr. Compos.* 26 (1) (2004) 31–39, [https://doi.org/10.1016/S0958-9465\(02\)00120-8](https://doi.org/10.1016/S0958-9465(02)00120-8).
- [45] K. Ganesan, K. Rajagopal, K. Thangavel, Rice husk ash blended cement: Assessment of optimal level of replacement for strength and permeability properties of concrete, *Constr. Build. Mater.* 22 (8) (2008) 1675–1683, <https://doi.org/10.1016/j.conbuildmat.2007.06.011>.
- [46] G.A. Habeeb, M.M. Fayyadh, Rice husk ash concrete: the effect of RHA average particle size on mechanical properties and drying shrinkage, *Aust. J. Basic Appl. Sci.* 3 (3) (2009) 1616–1622.
- [47] A.N. Givi, S.A. Rashid, F.N.A. Aziz, M.A.M. Salleh, Assessment of the effects of rice husk ash particle size on strength, water permeability and workability of binary blended concrete, *Constr. Build. Mater.* 24 (11) (2010) 2145–2150, <https://doi.org/10.1016/j.conbuildmat.2010.04.045>.
- [48] V. Srivastava, R. Kumar, V.C. Agarwal, P.K. Mehta, Effect of Silica Fume and Metakaolin combination on concrete, *Int. J. Civ. Struct. Eng.* 2 (3) (2012) 893–900.
- [49] Ş. Yazici, H.Ş. Arel, Effects of fly ash fineness on the mechanical properties of concrete, *Sadhana* 37 (3) (2012) 389–403.
- [50] (Sadhanā – a Vol. 37, Part 3, June 2012, pp. 389–403. c Indian Academy of Sciences).
- [51] N.K. Amudhavalli, J. Mathew, Effect of silica fume on strength and durability parameters of concrete, *Int. J. Eng. Sci. Technol.* 3 (1) (2012) 28–35.
- [52] V.M. Shelke, P. Pawde, R. Shrivastava, Effect of marble powder with and without silica fume on mechanical properties of concrete, *J. Mech. Civ. Eng.* 1 (1) (2012) 40–45.
- [53] D.K. Soni, J. Saini, Mechanical properties of high volume fly Ash (HVFA) and concrete subjected to evaluated 120 0 C temperature, *International Journal of Civil Engineering Research* 5 (3) (2014) 241–248.
- [54] M. Mahdikhani, A.A. Ramezaniapour, Mechanical properties and durability of self consolidating cementitious materials incorporating nano silica and silica fume, *Comput. Concrete* 14 (2) (2014) 175–191.
- [55] Vignesh G, Selwyn Babu J (2016) Effect of silica fume on properties of high strength concrete with recycled concrete aggregate. *Int J Sci Res.* <https://doi.org/10.1016/j.hbrcj.2014.06.002>.
- [56] Ngo, S. H., Huynh, T. P., Le, T. T. T., & Mai, N. H. T. (2018, June). Effect of high loss on ignition-fly ash on properties of concrete fully immersed in sulfate solution. In IOP conference series: materials science and engineering (Vol. 371, No. 1, p. 012007). IOP Publishing.
- [57] P.G. Asteris, P.B. Lourenço, C.A. Adami, P.C. Roussis, D.J. Armaghani, L. Cavalieri, C.E. Chalioris, M. Hajihassani, M.E. Lemonis, A.S. Mohammed, K. Pilakoutas, Revealing the nature of metakaolin-based concrete materials using Artificial Intelligence Techniques, *Constr. Build. Mater.* 322 (2021) 126500.
- [58] P.G. Asteris, M.E. Lemonis, T.-T. Le, K.D. Tsavdaridis, Evaluation of the ultimate eccentric load of rectangular CFSTs using advanced neural network modeling, *Eng. Struct.* 248 (2021) (2021), 113297, <https://doi.org/10.1016/j.engstruct.2021.113297>.
- [59] Asteris, P.G., Lourenço, P.B., Hajihassani, M., Adami, C.-E. N., Lemonis, M.E., Skentou, A.D., Marques, R., Nguyen, H., Rodrigues, H. and Varum, H. (2021). Soft computing based models for the prediction of masonry compressive strength, *Engineering Structures*, Volume 248, 113276, <https://doi.org/10.1016/j.engstruct.2021.113276>.
- [60] A. Mohammed, L. Burhan, K. Ghafor, W. Sarwar, W. Mahmood, Artificial neural network (ANN), M5P-tree, and regression analyses to predict the early age compression strength of concrete modified with DBC-21 and VK-98 polymers, *Neural Comput. Appl.* 33 (13) (2021) 7851–7873, <https://doi.org/10.1007/s00521-020-05525-y>.
- [61] A. Salih, S. Rafiq, P. Sihag, K. Ghafor, W. Mahmood, W. Sarwar, Systematic multiscale models to predict the effect of high-volume fly ash on the maximum compression stress of cement-based mortar at various water/cement ratios and curing times, *Measurement* 171 (2021), 108819, <https://doi.org/10.1016/j.measurement.2020.108819>.
- [62] A. Mohammed, S. Rafiq, P. Sihag, W. Mahmood, K. Ghafor, W. Sarwar, ANN, M5P-tree model, and nonlinear regression approaches to predict the compression strength of cement-based mortar modified by quicklime at various water/cement ratios and curing times, *Arabian J. Geosci.* 13 (22) (2020) 1–16, <https://doi.org/10.1007/s12517-020-06199-5>.
- [63] A. Mohammed, S. Rafiq, W. Mahmood, H. Al-Darkazalir, R. Noaman, W. Qadir, K. Ghafor, Artificial Neural Network and NLR techniques to predict the rheological properties and compression strength of cement past modified with nanoclay, *Ain Shams Eng. J.* 12 (2) (2021) 1313–1328, <https://doi.org/10.1016/j.asnj.2020.07.033>.
- [64] S.K. Rafiq, Modeling and statistical assessments to evaluate the effects of fly ash and silica fume on the mechanical properties of concrete at different strength ranges, *Journal of Building Pathology and Rehabilitation* 5 (1) (2020) 1–15.